Nucl. Phys. B 1006 (2024) 116631

Contents lists available at ScienceDirect

Nuclear Physics, Section B

journal homepage: www.elsevier.com/locate/nuclphysb

High Energy Physics – Phenomenology

New physics pathways from B processes ☆

Alessandra D'Alise [a], Giuseppe Fabiano [a], Domenico Frattulillo [a], Davide Iacobacci [a], Francesco Sannino [a,b,c,*], Pietro Santorelli [a,], Natascia Vignaroli [a,d]

[a] Dipartimento di Fisica "E. Pancini", Università di Napoli Federico II - INFN sezione di Napoli, Complesso Universitario di Monte S. Angelo Edificio 6, via Cintia, 80126 Napoli, Italy
[b] Scuola Superiore Meridionale, Largo S. Marcellino, 10, 80138 Napoli NA, Italy
[c] Quantum Theory Center (ħQTC), Danish-IAS, IMADA, Southern Denmark Univ., Campusvej 55, 5230 Odense M, Denmark
[d] Dipartimento di Matematica e Fisica "E. De Giorgi", Università del Salento and INFN Lecce, via per Arnesano, 73100 Lecce, Italy

ARTICLE INFO

Editor: Hong-Jian He

ABSTRACT

We re-consider recent measures of R_K and R_{K^*}, now compatible with the Standard Model expectations, as well as the results for the process BR($B_s \to \mu^+\mu^-$) alongside earlier determinations of $R_{D^{(*)}}$ and BR($B_c \to \tau\nu$). We provide analytic constraints on the associated Wilson coefficients in both the $b \to s$ and the $b \to c$ sectors. These allow us to estimate the scale of potential New Physics for generic extensions of the Standard Model. We then use the results to constrain the leptoquark landscape.

Contents

☆ Link to arXiv repository: https://arxiv.org/abs/2403.17614.

* Corresponding author.
E-mail address: sannino@qtc.sdu.dk (F. Sannino).

https://doi.org/10.1016/j.nuclphysb.2024.116631
Received 20 April 2024; Received in revised form 24 June 2024; Accepted 11 July 2024

Available online 25 July 2024

1. Introduction

Experimental tests at colliders of the Standard Model have crowned it as the golden standard of our understanding of fundamental interactions. However, the model is far from being satisfactory. From a theoretical standpoint, there is no underlying explanation for the gauge structure nor why we observe three matter generations, the Higgs sector is unnatural and the theory, in absence of gravity, develops an UV cutoff (Landau Pole) and there is yet no consensus on a consistent theory of quantum gravity and particle physics. On the experimental front, the Standard Model fails to explain the matter-anti matter asymmetry, it lacks a candidate for dark matter and does not address the origin of neutrino masses. It is therefore fair to say that we have so far established an excellent "Effective Model" of fundamental interactions and that sometime (hopefully) soon even collider experiments will provide clear indications on which extension should be considered as the new Standard Model.

Of course, any extension of the Standard Model will have to reproduce its successes at lower energies, and one can use this to narrow the pathways for new physics models. In our recent review [1] we laid the foundations for a general investigation of models of new physics stemming from experimental test of the Standard Model, from B physics to lepton $g-2$.

Given the experimental updates such as the ones about lepton-flavor universality [2,3] we re-analyze their impact on possible deviations from the Standard Model while also taking into account the anomalies in the R_{D^*} measurements [4] that we had omitted in [1]. Additionally we consider also the still significant deviations from the SM predictions in rare B meson decays [5–19]. In particular, we will consider the leptoquark landscape which has been often used in the literature to discuss new physics in the flavour sector either as elementary extensions of the Standard Model or as effective descriptions of some underlying composite dynamics. As we shall see, our estimates can be used to guide searches of new physics at present and future colliders.

The work is organized as follows. In Section 2 and 3 we re-analyse the experimental results and their impact on the associated theoretical effective description in terms of Wilson coefficients for $b\to c$ and $b\to s$ observables. An analytic study is performed for those observables that are less affected by hadronic physics contamination which are $R_{K^{(*)}}$, $R_{D^{(*)}}$, $\mathrm{BR}(B_s\to\mu^+\mu^-)$ and $\mathrm{BR}(B_c\to\tau\nu)$. We further compare the analytic results with numerical fits using FLAVIO [20] consolidating our results. Having gained information on the maximum deviation allowed by the Wilson coefficients we link them to time-honoured underlying models in Section 4 such as the Z' and different type of scalar and vector leptoquarks (LQ). Assuming our focus on models of new physics (NP) in which the new couplings are not too finely tuned, we show that to simultaneously accommodate Standard Model deviations in $R_{D^{(*)}}$, while respecting the constraints coming from $R_{K^{(*)}}$, one can employ the weak singlet scalar leptoquark S_1, with a mass in the TeV range. Additionally, our analysis suggests that alternative leptoquark models require large fine-tuned couplings to effectively account for both $b\to s$ and $b\to c$ data. Subsequently, we furnish bounds on the possible NP scales.

2. $b\to s$ flavour constraints

To explore NP emerging around the electroweak energy scale affecting the bottom to strange transitions involving leptons one is led to introduce the following class of effective operators

$$\mathcal{O}_{b_X\ell_Y}=(\bar{s}\gamma_\mu P_X b)(\bar{\ell}\gamma_\mu P_Y\ell)\,, \tag{1}$$

which can be written as $\mathrm{SU}(2)_L$-invariant operators. A more general discussion can be found in [21–23]. These operators are incorporated in the following effective Hamiltonian

$$\mathscr{H}_{\mathrm{eff}}=-V_{tb}V_{ts}^*\frac{\alpha_{\mathrm{em}}}{4\pi v^2}\sum_{\ell,X,Y}C_{b_X\ell_Y}\mathcal{O}_{b_X\ell_Y}\ +\mathrm{h.c.}\,, \tag{2}$$

where the sum runs over leptons $\ell=\{e,\mu,\tau\}$ and over their chiralities $X,Y=\{L,R\}$. Additionally, it is convenient to define dimensionless coefficients C_I related to the dimensionful c_I coefficients appearing in the equivalent Lagrangian formulation

$$\mathscr{L}_{\mathrm{eff}}=\sum_{\ell,X,Y}c_{b_X\ell_Y}\mathcal{O}_{b_X\ell_Y}\ ,\ \text{with}\quad c_I=V_{tb}V_{ts}^*\frac{\alpha_{\mathrm{em}}}{4\pi v^2}C_I\ , \tag{3}$$

where $V_{ts}=-0.0412\pm0.0006$ and $v=(2\sqrt{2}G_{\mathrm{F}})^{-1/2}=174$ GeV is the Higgs vacuum expectation value and G_{F} the Fermi constant.

2.1. Applications to $R_{K^{(*)}}$ and $BR(B_s\to\mu^+\mu^-)$

As main applications of the formalism above we start by considering the well known R_K and R_{K^*} ratios [6–8,12]

$$R_K=\frac{\mathrm{BR}\left(B^+\to K^+\mu^+\mu^-\right)}{\mathrm{BR}\left(B^+\to K^+e^+e^-\right)},\quad R_{K^*}=\frac{\mathrm{BR}\left(B\to K^*\mu^+\mu^-\right)}{\mathrm{BR}\left(B\to K^*e^+e^-\right)}. \tag{4}$$

These quantities are known to be excellent tests of lepton flavour universality since they are constructed to reduce QCD-related uncertainties [24]. Therefore, together with the $B_s \to \mu^+\mu^-$ branching ratio [9,13,14] are hadronic insensitive [25] quantities. Here, 'hadronic insensitive' (HI) [25] refers to the fact that the related observables have at most few percent QCD-induced theoretical errors.

The latest experimental results for $R_{K^{(*)}}$ read [2,3]:

$$R_K = 0.994^{+0.090}_{-0.082}(\text{stat})^{+0.029}_{-0.027}(\text{syst}) \quad \text{with} \quad q^2 \in [0.1, 1.1]\,\text{GeV}^2\,, \tag{5}$$

$$R_{K^*} = 0.927^{+0.093}_{-0.087}(\text{stat})^{+0.036}_{-0.035}(\text{syst}) \quad \text{with} \quad q^2 \in [0.1, 1.1]\,\text{GeV}^2\,, \tag{6}$$

$$R_K = 0.949^{+0.042}_{-0.041}(\text{stat})^{+0.022}_{-0.022}(\text{syst}) \quad \text{with} \quad q^2 \in [1.1, 6]\,\text{GeV}^2\,, \tag{7}$$

$$R_{K^*} = 1.027^{+0.072}_{-0.068}(\text{stat})^{+0.027}_{-0.026}(\text{syst}) \quad \text{with} \quad q^2 \in [1.1, 6]\,\text{GeV}^2\,. \tag{8}$$

At high q^2 one can neglect the lepton masses and the formulae for R_K and R_{K^*} simplify to[1]

$$R_K = \frac{|C_{b_{L+R}\mu_{L-R}}|^2 + |C_{b_{L+R}\mu_{L+R}}|^2}{|C_{b_{L+R}e_{L-R}}|^2 + |C_{b_{L+R}e_{L+R}}|^2}\,, \tag{9}$$

$$R_{K^*} = \frac{(1-p)(|C_{b_{L+R}\mu_{L-R}}|^2 + |C_{b_{L+R}\mu_{L+R}}|^2) + p\left(|C_{b_{L-R}\mu_{L-R}}|^2 + |C_{b_{L-R}\mu_{L+R}}|^2\right)}{(1-p)(|C_{b_{L+R}e_{L-R}}|^2 + |C_{b_{L+R}e_{L+R}}|^2) + p\left(|C_{b_{L-R}e_{L-R}}|^2 + |C_{b_{L-R}e_{L+R}}|^2\right)}\,, \tag{10}$$

where $p \approx 0.86$ is the "polarisation fraction" [26–28], that is defined as

$$p = \frac{g_0 + g_\parallel}{g_0 + g_\parallel + g_\perp}\,. \tag{11}$$

The g_i are the contributions to the decay rate (integrated over the intermediate bin) of the different helicities of the K^*. The index i distinguishes the various helicities: longitudinal ($i = 0$), parallel ($i = \parallel$) and perpendicular ($i = \perp$).
We also use the notation [1,25]:

$$C_{b_{L\pm R}\ell_Y} \equiv C_{b_L\ell_Y} \pm C_{b_R\ell_Y}\,, \quad C_{b_{L+R}\ell_{L\pm R}} \equiv C_{b_L\ell_L} + C_{b_R\ell_L} \pm C_{b_L\ell_R} \pm C_{b_R\ell_R}\,. \tag{12}$$

The coefficients $C_{b_X\ell_Y}$ are linked to C_9 and C_{10} via

$$2C_9 = C_{b_L\ell_{L+R}}\,, \quad 2C_{10} = -C_{b_L\ell_{L-R}}\,, \quad 2C_9' = C_{b_R\ell_{L+R}}\,, \quad 2C_{10}' = -C_{b_R\ell_{L-R}}\,. \tag{13}$$

We split the coefficients into the sum of the Standard Model contribution and the beyond Standard Model one via

$$C_{b_X\ell_Y} = C^{SM}_{b_X\ell_Y} + C^{BSM}_{b_X\ell_Y}\,. \tag{14}$$

We use the Standard Model values given in [1,25] to numerically specify expressions (9)-(10): $C^{SM}_{b_L\ell_L} = 8.64$ and $C^{SM}_{b_L\ell_R} = -0.18$, while $C^{SM}_{b_R\ell_X} = 0$ for $X = L, R$.
We assume that possible NP corrections occur in the muonic Wilson coefficients (i.e. $C^{BSM}_{b_Xe_Y} = 0$), implying Lepton Flavor Universality Violation (LFUV). Of course, NP effects could appear in other sectors as well (see e.g. [29,30]). However, experimentally muons are easier to monitor and therefore we focus on this possibility. Fig. 1 is the update of Fig. 3 in [1,25] and describes the effects on R_{K^*} and R_K obtained switching on one NP Wilson coefficient at a time. The recent experimental measurements are exemplified at one and two sigma by the green q^2 bin $[1.1, 6]\,\text{GeV}^2$ and dark-grey q^2 bin $[0.1, 1.1]\,\text{GeV}^2$ crosses. Substituting in (9)-(10) the SM values for the Wilson coefficients, we obtain

$$\begin{aligned} R_K =& 1 + 0.231[Re(C^{BSM}_{b_L\mu_L}) + Re(C^{BSM}_{b_R\mu_L})] - 0.005[Re(C^{BSM}_{b_L\mu_R}) + Re(C^{BSM}_{b_R\mu_R})] + \\ &+ 0.013\{[Re(C^{BSM}_{b_L\mu_L}) + Re(C^{BSM}_{b_R\mu_L})]^2 + [Re(C^{BSM}_{b_L\mu_R}) + Re(C^{BSM}_{b_R\mu_R})]^2\}\,, \\ R_{K^*} - R_K =& -0.398\,Re(C^{BSM}_{b_R\mu_L}) + 0.008\,Re(C^{BSM}_{b_R\mu_R}) \\ &- 0.046[Re(C^{BSM}_{b_L\mu_L})Re(C^{BSM}_{b_R\mu_L})) + Re(C^{BSM}_{b_L\mu_R})Re(C^{BSM}_{b_R\mu_R})]\,. \end{aligned} \tag{15}$$

Another relevant clean observable for studying constraints on the NP coefficient is the branching ration $\text{BR}(B_s \to \mu^+\mu^-)$, which in terms of NP coefficients reads

$$\text{BR}(B_s \to \mu^+\mu^-) = \text{BR}(B_s \to \mu^+\mu^-)_{\text{SM}} \left| \frac{C_{b_{L-R}\mu_{L-R}}}{C^{\text{SM}}_{b_{L-R}\mu_{L-R}}} \right|^2\,, \tag{16}$$

[1] It is worth to mention that the analytic formulas given in Eqs. (9), and (10) provide a less precise approximation for the lower bin $[0.1, 1.1]$. Nevertheless, it is important to observe that measurements of the lower q^2 interval are associated with a higher level of uncertainty compared to the higher bin.

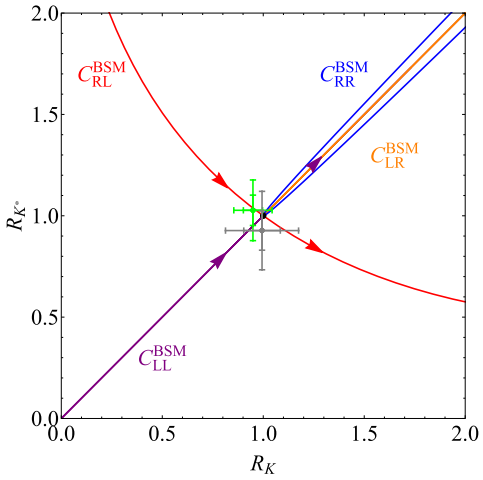

Fig. 1. Quantitative behaviour of R_K vs R_{K^*} as in (9)-(10), normalised by their SM value, obtained by switching on one NP coefficient at a time. The experimental values for the $[1.1, 6]\,\mathrm{GeV}^2$ bin (in green) and for the $[0.1, 1.1]\,\mathrm{GeV}^2$ bin (in grey) are shown with 1σ and 2σ error bars. The experimental values are compatible with the SM in the 2-sigma range, signalling values of the NP coefficients close to 0.

with $\mathrm{BR}(B_s \to \mu^+\mu^-)_{\mathrm{SM}} = (3.66 \pm 0.14) \times 10^{-9}$. Following the most recent measurement by the CMS collaboration [31], the experimental value, as reported in [32], for the branching ratio $\mathrm{BR}(B_s \to \mu^+\mu^-)_{\mathrm{exp}}$ is now $(3.28 \pm 0.26) \times 10^{-9}$. This measurement is now even closer to the Standard Model prediction. Inserting the numerical values for the SM Wilson coefficients the above becomes

$$\begin{aligned}\frac{\mathrm{BR}(B_s \to \mu^+\mu^-)}{\mathrm{BR}(B_s \to \mu^+\mu^-)_{\mathrm{SM}}} &= 1 + 0.227[Re(C^{BSM}_{b_L\mu_L}) + Re(C^{BSM}_{b_R\mu_R}) - Re(C^{BSM}_{b_L\mu_R}) - Re(C^{BSM}_{b_R\mu_L})] + \\ &+ 0.013[Re(C^{BSM}_{b_L\mu_L}) + Re(C^{BSM}_{b_R\mu_R}) - Re(C^{BSM}_{b_L\mu_R}) - Re(C^{BSM}_{b_R\mu_L})]^2\end{aligned} \tag{17}$$

As a preliminary step, we consider the 2-σ interval for the experimental values presented above in order to obtain constraints on the Wilson coefficients. As mentioned earlier the values of R_K and R_{K^*} in the lower q^2 interval are associated with a higher level of uncertainty compared to the higher bin. As a result the relevant constraint stems from the q^2 bin $[1.1, 6]\mathrm{GeV}^2$, as well as from the $\mathrm{BR}(B_s \to \mu^+\mu^-)$.
When switching on one real Wilson coefficient at a time, our analytical analysis, at the 2-σ level, yields the following constraints:

$$C^{\mathrm{BSM}}_{b_L\mu_L} \in [-0.53, 0.19]\,, \tag{18}$$

$$C^{\mathrm{BSM}}_{b_L\mu_R} \in [-0.46, 1.51]\,, \tag{19}$$

$$C^{\mathrm{BSM}}_{b_R\mu_L} \in [-0.46, 0.19]\,, \tag{20}$$

$$C^{\mathrm{BSM}}_{b_R\mu_R} \in [-1.51, 0.46]\,. \tag{21}$$

These intervals provide a first idea of the acceptable ranges for the associated Wilson coefficients, taking into account uncertainties at 2-σ confidence level. We have also considered the imaginary parts of the Wilson coefficients, but we will concentrate on the real parts since these are preferred by the data.

2.2. Fit analysis

So far we examined the essential features of the HI observables, laying the groundwork for our expectations in the comparisons with experimental data.
Building upon the analysis presented in [1,25], this section utilises the FLAVIO toolkit [20] to revise the outcomes of the fitting procedure, refining the values of the Wilson NP coefficients to optimally align with the available dataset. In the initial phase of our analysis, we concentrate exclusively on the HI set of observables. Following this, we estimate the influence of the 'Hadronic Sensitive' (HS) observables and subsequently incorporate them into a unified global fitting procedure.
In Table 1, we provide a concise overview of the updated outcomes obtained from the fitting procedure, focusing on the scenario where individual Wilson coefficients are turned on one at a time. To ensure a comprehensive update of the findings presented in [1], we extend our analysis to include situations where NP effects are assumed in the electron sector only.

The obtained results align with the analytic investigation presented in section 2.1. The overall deviation from the SM is significantly mitigated with respect to previous results [1,23,25,33–45]. This is to be expected because the recent experimental measurements align well with the SM predictions. In fact, the muon Wilson coefficients are now in agreement with the SM within a 1.2σ confidence level. As for the muon case, the electron sector fit showes compatibility with the SM with a significance of 0.7σ. For completeness, we show in Table 2 the results of 1-parameter fits in the vector-axial basis.

Table 1
Best fits turning on a single operator at a time in the chiral basis, using the 'hadronic insensitive' observables 'HI', the 'hadronic sensitive' observables 'HS', or all the observables 'all'. The full list of observables can be found in Appendix A.

	New physics in the muon sector (Chiral basis)								
	Best-fit			1-σ range			$\sqrt{\chi^2_{\rm SM} - \chi^2_{\rm best}}$		
	HI	*HS*	*all*	*HI*	*HS*	*all*	*HI*	*HS*	*all*
$C^{\rm BSM}_{b_L\mu_L}$	−0.15	−1.31	−0.33	−0.05 −0.25	−1.05 −1.56	−0.24 −0.42	1.1	4.1	2.8
$C^{\rm BSM}_{b_L\mu_R}$	0.40	−0.66	−0.25	0.64 0.16	−0.47 −0.85	−0.10 −0.40	1.2	2.6	1.7
$C^{\rm BSM}_{b_R\mu_L}$	−0.05	0.08	−0.04	0.05 −0.15	0.19 −0.03	0.04 −0.12	0.3	0.5	0.3
$C^{\rm BSM}_{b_R\mu_R}$	−0.38	0.30	0.05	−0.13 −0.63	0.52 0.18	0.20 −0.10	1.1	1.6	0.2
	New physics in the electron sector (Chiral basis)								
	Best-fit			1-σ range			$\sqrt{\chi^2_{\rm SM} - \chi^2_{\rm best}}$		
	HI	*HS*	*all*	*HI*	*HS*	*all*	*HI*	*HS*	*all*
$C^{\rm BSM}_{b_Le_L}$	0.10	0.94	0.14	0.21 −0.01	1.45 0.43	0.25 0.03	0.7	1.2	0.9
$C^{\rm BSM}_{b_Le_R}$	−0.17	−2.71	−0.70	1.03 −1.37	−1.03 −1.73	−0.11 −1.29	0.1	1.3	0.6
$C^{\rm BSM}_{b_Re_L}$	0.14	−3.87	0.15	0.25 0.03	−2.86 −4.88	0.26 0.04	0.9	1.4	1.0
$C^{\rm BSM}_{b_Re_R}$	−1.22	−3.94	−1.43	−0.59 −1.85	−2.92 −4.96	0.08 −2.94	0.9	1.4	1.1

In summary, when focusing the analysis on the specific subset of HI observables R_K, R_{K^*} and BR($B_s \to \mu^+\mu^-$), the overall results indicate a compatibility with the Standard Model within nearly a 1σ level.
Nevertheless, a significant deviation in the muon sector persists, originating from the HS observables. In the electron sector, however, one observes a reduced deviation from the SM which now hovers around 1σ. This is to be expected since the majority of HS observables deviating from the SM involve muons.
We finally combine HS and HI observables in a global fit. When considering the single coefficient turned on, in the muon sector, we conclude that the results favour a deviation in the SM in $C^{\rm BSM}_{b_L\mu_L}$ as well as $C^{\rm BSM}_{b_L\mu_R}$, with a larger significance for the left-handed muon coefficient than the right-handed one. Meanwhile, we observe that $C^{\rm BSM}_{b_R\mu_L}$ and $C^{\rm BSM}_{b_R\mu_R}$ remain compatible with the SM value, as do all the electronic coefficients.

Then, we proceed with a comprehensive fit involving multiple Wilson coefficients. Given the reduced sensitivity of our observables to electronic coefficients, we exclusively focus on the muonic operators. When turning on four BSM Wilson coefficients at once, the results of the global fit are:

$$\begin{aligned} C^{\rm BSM}_{b_L\mu_L} &= -0.65 \pm 0.10\,, \\ C^{\rm BSM}_{b_L\mu_R} &= -0.93 \pm 0.09\,, \quad \chi^2_{SM} = 264.99\,, \\ C^{\rm BSM}_{b_R\mu_L} &= 0.20 \pm 0.15\,, \quad \tilde{\chi}^2 = 246.77\,. \\ C^{\rm BSM}_{b_R\mu_R} &= -0.16 \pm 0.28\,. \end{aligned} \qquad \rho = \begin{pmatrix} 1 & 0.15 & -0.36 & -0.29 \\ -0.15 & 1 & 0.28 & 0.39 \\ -0.36 & 0.28 & 1 & 0.83 \\ -0.29 & 0.39 & 0.83 & 1 \end{pmatrix}. \tag{22}$$

We report the reduced chi-square:

$$\frac{\chi^2_{SM}}{\#\ \text{d.o.f.}} = 0.985\,, \qquad \frac{\tilde{\chi}^2}{\#\ \text{d.o.f.}} = 0.931\,. \tag{23}$$

When comparing the χ^2 values, we find a deviation from the SM at the 4.3σ level. However, upon using the "Pull" value, as defined in [46]:

$$\text{Pull} = \sqrt{\text{CDF}_1^{-1}(\text{CDF}_{N_{par}}(\chi^2_{SM} - \tilde{\chi}^2))}\,, \tag{24}$$

Table 2
Best fits turning on a single operator at a time in the vector-axial basis, using the 'hadronic insensitive' observables 'HI', the 'hadronic sensitive' observables 'HS', or all the observables 'all'.

	New physics in the muon sector (Vector Axial basis)								
	Best-fit			1-σ range			$\sqrt{\chi^2_{\rm SM} - \chi^2_{\rm best}}$		
	HI	*HS*	*all*	*HI*	*HS*	*all*	*HI*	*HS*	*all*
$C^{\rm BSM}_{9,\mu}$	−0.12	−0.94	−0.49	−0.24 0.00	−0.82 −1.06	−0.39 −0.59	0.7	4.9	3.6
$C^{\rm BSM}_{10,\mu}$	0.14	−0.23	0.16	0.22 0.06	0.36 0.09	0.23 0.09	1.3	1.2	1.6
$C'^{\rm BSM}_{9,\mu}$	−0.01	0.20	−0.03	0.07 −0.09	0.33 0.07	0.05 −0.11	0.9	1.1	0.3
$C'^{\rm BSM}_{10,\mu}$	−0.15	0	0.03	−0.26 −0.04	0.08 −0.08	0.08 −0.02	0.1	0	0.3
	New physics in the electron sector (Vector Axial basis)								
	Best-fit			1-σ range			$\sqrt{\chi^2_{\rm SM} - \chi^2_{\rm best}}$		
	HI	*HS*	*all*	*HI*	*HS*	*all*	*HI*	*HS*	*all*
$C^{\rm BSM}_{9,e}$	0.12	1.01	0.15	0.24 0.00	1.55 0.47	0.26 0.04	0.7	1.4	1.0
$C^{\rm BSM}_{10,e}$	−0.09	−0.79	−0.12	0.01 −0.19	−0.36 −1.21	−0.02 −0.22	0.6	1.2	0.9
$C'^{\rm BSM}_{9,e}$	0.15	0.20	0.16	0.27 0.03	0.33 0.07	0.27 0.05	0.9	1.4	1.0
$C'^{\rm BSM}_{10,e}$	−0.14		−0.14	−0.04 −0.24		−0.40 −0.24	0.9		1.0

we also take into account the number of parameters switched on. Here, CDF_n stands for the cumulative distribution function of a χ^2-distributed random variable with n degrees of freedom, and N_{par} is the number of fitted parameters. Using (24), the discrepancy with the SM is revealed at a slightly reduced significance level of $3.3\,\sigma$.

Interestingly, we observe that the results in (22) agree within a σ from the findings presented in [1], when the global fit was performed already assuming $R_K = R_{K^*} = 1$ long before the latest experimental values were available and before any other successive investigation.

2.3. Leptoquark motivated fit scenarios

To conclude this section, we now analyse the possibility of NP scenarios involving the simultaneous activation of two Wilson coefficients. As we shall review in section 4, LQ are primary examples of these type of models with the scalar $S_1 = (\bar{\mathbf{3}}, \mathbf{1}, 1/3)$ and vector $U_1 = (\mathbf{3}, \mathbf{1}, 2/3)$ LQs being the relevant ones here because they turn on the following NP coefficients:

$$S_1 : C^{\rm BSM}_{b_L\mu_L}, C^{\rm BSM}_{b_L\mu_R} \,, \tag{25}$$

$$U_1 : C^{\rm BSM}_{b_L\mu_L}, C^{\rm BSM}_{b_R\mu_R} \,. \tag{26}$$

The associated contour plots are given in Fig. 2, corresponding to the fitted results:

$$S_1 : \begin{cases} C^{\rm BSM}_{b_L\mu_L} &= -0.52 \pm 0.12 \,, \\ C^{\rm BSM}_{b_L\mu_R} &= -0.64 \pm 0.14 \,, \end{cases} \qquad \text{Pull} = 3.3\sigma \quad \rho = \begin{pmatrix} 1 & 0.54 \\ 0.54 & 1 \end{pmatrix} \,, \tag{27}$$

$$U_1 : \begin{cases} C^{\rm BSM}_{b_L\mu_L} &= -0.31 \pm 0.09 \,, \\ C^{\rm BSM}_{b_R\mu_R} &= 0.21 \pm 0.05 \,, \end{cases} \qquad \text{Pull} = 1.9\sigma \quad \rho = \begin{pmatrix} 1 & -0.47 \\ -0.47 & 1 \end{pmatrix} \,. \tag{28}$$

We note that the S_1 model is favoured over the U_1 one when we consider both coefficients turned on simultaneously.

3. $b \to c$ flavour sector

So far, we concentrated on Flavor Changing Neutral Currents (FCNC) process $b \to s\ell^+\ell^-$, it is therefore time to tackle the Flavor Changing Charged Currents (FCCC) sector via the decays $b \to c\ell^-\nu_\ell$. For these, the most general low-energy effective Hamiltonian including operators up to dimension six is:

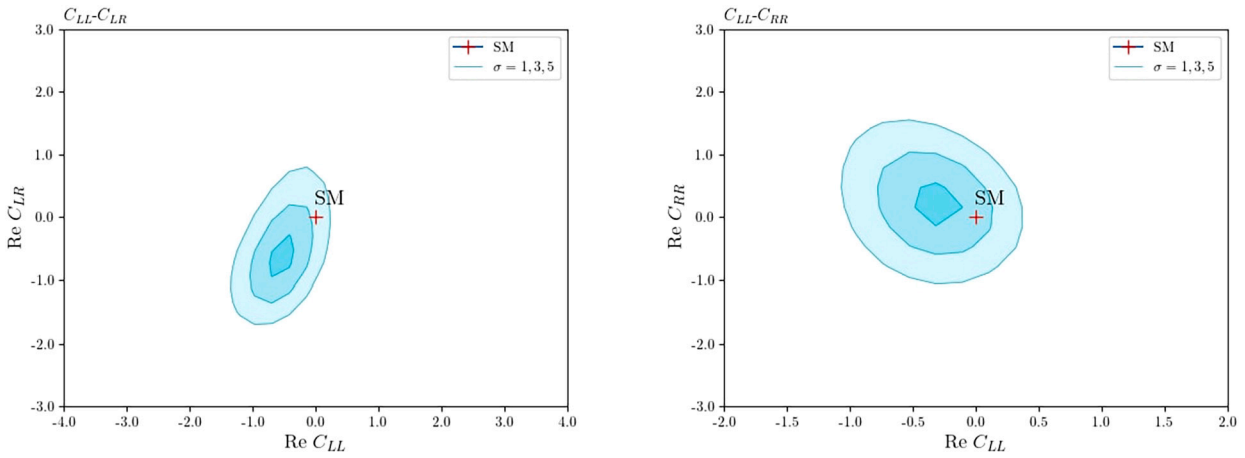

Fig. 2. Contour plots corresponding to the LQ motivated scenarios where we turn on 2 Wilson coefficients at a time, while fixing the remaining coefficients to zero. We use the full list of observables given in Appendix A and present the contour plots corresponding to the 1, 3, and 5-σ confidence levels, along with the corresponding SM value.

$$\mathscr{H}_{\text{eff}} = -V_{cb}\frac{\alpha_{\text{em}}}{4\pi v^2}[(1+C_{V_L})\mathcal{O}_{V_L} + C_{V_R}\mathcal{O}_{V_R} + C_{S_L}\mathcal{O}_{S_L} + C_{S_R}\mathcal{O}_{S_R} + C_T\mathcal{O}_T + \text{h.c.}]\,, \tag{29}$$

with

$$\begin{aligned}
\mathcal{O}^{\ell}_{V_L} &= (\bar{c}_L\gamma^\mu b_L)(\bar{\ell}_L\gamma_\mu \nu_{\ell L})\,,\\
\mathcal{O}^{\ell}_{V_R} &= (\bar{c}_R\gamma^\mu b_R)(\bar{\ell}_L\gamma_\mu \nu_{\ell L})\,,\\
\mathcal{O}^{\ell}_{S_L} &= (\bar{c}_L b_R)(\bar{\ell}_R \nu_{\ell L})\,,\\
\mathcal{O}^{\ell}_{S_R} &= (\bar{c}_R b_L)(\bar{\ell}_R \nu_{\ell L})\,,\\
\mathcal{O}^{\ell}_{T} &= (\bar{c}_R\sigma^{\mu\nu} b_L)(\bar{\ell}_R \sigma_{\mu\nu}\nu_{\ell L})\,.
\end{aligned} \tag{30}$$

The NP contributions, differently from the FCNC case, are directly encoded in the Wilson coefficients (WCs), denoted as C_X. One can envision including operators accounting for contributions stemming from right-handed neutrinos, [47–49]. These, however, would go beyond the scope of this work which is to keep the level of model building minimal. We now turn to contributions stemming from the tau sector only.

3.1. Current status of the $b \to c$ observables

The semi-tauonic decays of B mesons, specifically $B \to D^{(*)}\tau\overline{\nu}$, are crucial processes for probing lepton flavor universality violation (LFUV), complementing the investigation of $B \to K^{(*)}\ell\ell$ discussed in the preceding section. The ratios

$$R_D = \frac{\text{BR}(B \to D\,\tau\,\overline{\nu}_\tau)}{\text{BR}(B \to D\,\ell\,\overline{\nu}_\ell)}, \tag{31}$$

$$R_{D^*} = \frac{\text{BR}(B \to D^*\tau\,\overline{\nu}_\tau)}{\text{BR}(B \to D^*\ell\,\overline{\nu}_\ell)}, \quad \ell = e, \mu, \tag{32}$$

have been computed with high precision. This precision is achieved through the remarkable suppression of hadronic uncertainties associated with the strong interaction in the $B \to D^{(*)}$ transitions.

The experimental measurements, as detailed in Table 3, consistently reveal deviations from Standard Model predictions. Notably, the characteristic pattern is that the experimental values of $R_{D^{(*)}}$ exceed the SM predictions, implying a systematic violation of lepton flavor universality (LFU). In Table 3, we provide a concise overview of the current status of independent measurements of R_D and R_{D^*} conducted by various collaborations. We also include the latest result on R_{D^*} from Belle II from the recent presentation in [50]. In addition to the ratios R_D and R_{D^*}, significant constraints arise from the B_c meson branching ratio $\text{BR}(B_c \to \tau\nu_\tau)$. The upper bound on the branching ratio $\text{BR}(B_c \to \tau\nu_\tau)$ is given as $\text{BR}(B_c \to \tau\nu_\tau) \leq 0.3$ according to [51]. Alternatively, a more conservative limit of 0.6 is suggested in [46], while a more stringent bound of 0.1, based on LEP data, is presented in [52].

In our analysis, we also consider the measurement of the D^* meson longitudinal polarisation fraction, denoted as $F_L^{D^*}$, with a value of $0.60 \pm 0.08 \pm 0.04$, as reported by the Belle collaboration [53]. This result is in agreement within approximately 1.7σ with the SM prediction.

Table 3
Current status of the independent experimental $R_{D^{(*)}}$ measurements. The first and second errors are statistical and systematic, respectively.

Experiment	R_{D^*}	R_D	Correlation
BaBar [54,55]	$0.332 \pm 0.024 \pm 0.018$	$0.440 \pm 0.058 \pm 0.042$	−0.27
Belle [56]	$0.293 \pm 0.038 \pm 0.015$	$0.375 \pm 0.064 \pm 0.026$	−0.49
Belle [57,58]	$0.270 \pm 0.035^{+0.028}_{-0.025}$	–	–
Belle [59,60]	$0.283 \pm 0.018 \pm 0.014$	$0.307 \pm 0.037 \pm 0.016$	−0.51
LHCb [61]	$0.281 \pm 0.018 \pm 0.024$	$0.441 \pm 0.060 \pm 0.066$	−0.43
LHCb [62]	$0.257 \pm 0.012 \pm 0.018$	–	–
Belle II [50]	$0.267^{+0.041+0.028}_{-0.039-0.033}$	–	–
World average [4]	0.284 ± 0.012	0.357 ± 0.029	−0.37

3.2. Analysis of the $b \to c$ observables

Using the effective Hamiltonian from Eq. (29), where the NP Wilson coefficients are defined at the renormalisation scale $\mu = \mu_b = 4.18\,\text{GeV}$, we employ the updated numerical formulas provided in [63]:

$$\frac{R_D}{R_D^{SM}} = \left|1 + C_{V_L} + C_{V_R}\right|^2 + 1.01\left|C_{S_R} + C_{S_L}\right|^2 + 0.84\left|C_T\right|^2 + 1.49\,Re[(1 + C_{V_L})(C^*_{S_R} + C^*_{S_L})] + 1.08\,Re[(1 + C_{V_L} + C_{V_R})C^*_T]\,, \tag{33}$$

$$\frac{R_{D^*}}{R_{D^*}^{SM}} = \left|1 + C_{V_L}\right|^2 + \left|C_{V_R}\right|^2 + 0.04\left|C_{S_L} - C_{S_R}\right|^2 + 16.0\left|C_T\right|^2 - 0.11\,Re\left[\left(1 + C_{V_L} - C_{V_R}\right)\left(C^*_{S_L} - C^*_{S_R}\right)\right] - 1.83\,Re\left[(1 + C_{V_L})C^*_{V_R}\right] - 5.17\,Re\left[\left(1 + C_{V_L}\right)C^*_T\right] + 6.60\,Re\left[C_{V_R}C^*_T\right]\,, \tag{34}$$

$$\frac{F_L^{D^*}}{F_{L,SM}^{D^*}} = \left(\frac{R_{D^*}}{R_{D^*}^{SM}}\right)^{-1}\left(\left|1 + C_{V_L} - C_{V_R}\right|^2 + 0.08\left|C_{S_L} - C_{S_R}\right|^2 + 6.90\left|C_T\right|^2 - 0.25\,Re\left[\left(1 + C_{V_L} - C_{V_R}\right)\left(C^*_{S_L} - C^*_{S_R}\right)\right] - 4.30\,Re\left[\left(1 + C_{V_L} - C_{V_R}\right)C^*_T\right]\right)\,, \tag{35}$$

$$\frac{\text{BR}(B_c^+ \to \tau^+ \nu_\tau)}{\text{BR}(B_c^+ \to \tau^+ \nu_\tau)_{SM}} = \left|1 + C_{V_L} - 4.35(C_{S_L} - C_{S_R})\right|^2\,. \tag{36}$$

The SM values that we used for these quantities are given by [4,63]

$$R_D^{SM} = 0.298\;\;,\quad R_{D^*}^{SM} = 0.254\,,\quad F_L^{D^*} = 0.464\,,\quad \text{BR}(B_c^+ \to \tau^+ \nu_\tau)_{SM} = 0.022\,. \tag{37}$$

Using the expressions for R_D and R_{D^*}, we illustrate in Fig. 3 the parametric curves corresponding to the single NP Wilson coefficient in the $R_D - R_{D^*}$ plane, along with the current experimental world average reported in Table 3.

Using the experimental values for the observables in Eqs. (33)–(36) and considering the 2-σ interval, we establish constraints on the Wilson coefficients when turning on a single coefficient at a time. We also explore scenarios motivated by LQ models, defined by the relations $C_{S_L}(\Lambda_{LQ}) = +4C_T(\Lambda_{LQ})$ and $C_{S_L}(\Lambda_{LQ}) = -4C_T(\Lambda_{LQ})$, at the LQ scale $\Lambda_{LQ} \approx 2\,\text{TeV}$. After accounting for the renormalisation group (RG) running from Λ_{LQ} to μ_b, these relations translate into $C_{S_L}(\mu_b) = 8.4C_T(\mu_b)$ and $C_{S_L}(\mu_b) = -8.9C_T(\mu_b)$ respectively [63,64]. The constraints at μ_b are:

$$C_{V_L} \in [0.01, 0.10]\,, \tag{38}$$

$$C_{S_R} \in [0.20, 0.23]\,, \tag{39}$$

$$C_{S_L} = -8.9C_T \in [0.05, 0.24]\,. \tag{40}$$

As shown in Fig. 3, the curve corresponding to $C_{S_L}(\Lambda_{LQ}) = +4C_T(\Lambda_{LQ})$ fails to explain the experimental data at the $2-\sigma$ level. It is worth mentioning that, even when considering both C_{S_L} and C_T individually, we are unable to reconcile the data. Therefore, we refrained from including the corresponding parametric curves explicitly in the figure.

It is also relevant to consider the scenario where purely imaginary values are allowed for the LQ-motivated coefficients. In this case, we find:

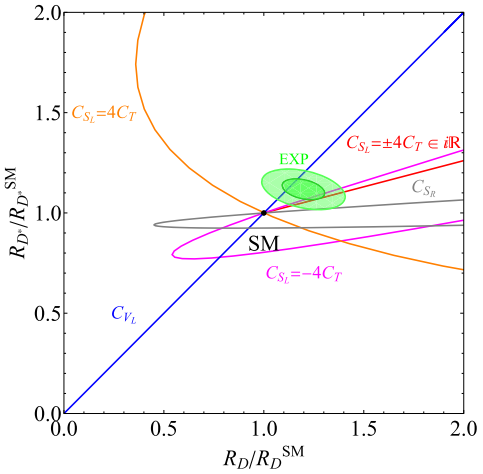

Fig. 3. Quantitative behaviour of R_D vs R_D^*, normalised by their SM value, obtained by switching on one NP coefficient at a time. We present the current experimental contours at 1 and 2-σ, delineated by darker and lighter green regions, respectively. The conditions $C_{S_L} = \pm 4C_T$ are imposed at 2 TeV and we provide the parametric curves after accounting for the RG running to the low energy scale μ_b.

Table 4
Best fits at the scale μ_b turning on a single operator at a time using the 'hadronic insensitive' observables 'HI' or all the observables 'all'. In analogy with the analysis of $b \to s$ data, here with HI observables we refer to Eqs. (33)–(36). The full list of observables can be found in Appendix A.

	New physics in the tau sector					
	Best-fit		1-σ range		$\sqrt{\chi^2_{SM} - \chi^2_{best}}$	
	HI	*all*	*HI*	*all*	*HI*	*all*
C_{V_L}	0.08	0.08	0.09 0.07	0.09 0.07	4.3	4.8
C_{V_R}	−0.06	−0.07	−0.04 −0.08	−0.05 −0.09	2.0	2.7
C_{S_L}	0.16	0.16	0.20 0.12	0.20 0.12	2.6	2.8
C_{S_R}	0.19	0.20	0.22 0.16	0.23 0.17	3.8	4.1
C_T	−0.03	−0.03	0.03 −0.09	0.02 −0.08	3.5	4.0

$$|\mathrm{ImC_{S_L}}| = 8.9|\mathrm{ImC_T}| \in [0.31, 0.62]\ , \tag{41}$$

$$|\mathrm{ImC_{S_L}}| = 8.4|\mathrm{ImC_T}| \in [0.30, 0.62]\ . \tag{42}$$

3.3. Fit analysis

We employ the FLAVIO package [20] to perform a fitting analysis of the Wilson coefficients at the scale μ_b to match the experimental data.

In order to see how NP scenarios improve the fit, especially when turning on more than one coefficient at a time, we use the "Pull" value defined in Eq. (24), which is expressed in terms of standard deviations σ [46]. Similar to our approach in the $b \to s$ sector, our initial analysis focuses solely on the observables defined in Eqs. (33)–(36). Also in this case we refer to these observables as "hadronic insensitive" as they are characterised by a strong suppression of hadronic uncertainties and thus predicted in the SM with an error up to few percent. Subsequently, we extend our analysis to include the effects of all available data summarised in Tables (8 – 10).

We systematically turn on each Wilson coefficient individually, assuming real values. Our results in Table 4 align with those reported in [63] within a 1-σ level. We notice a preference for NP coming from a nonzero value of the C_{V_L} Wilson coefficient with a significance of 4.3σ.

Upon allowing the Wilson coefficients to take on complex values, a significant improvement is observed in the fitting for C_{V_R} and C_{S_L}, while no enhancement is obtained for C_{V_L}, C_{S_R}, and C_T. When considering the set of observables given in Eqs. (33)–(36), the best fits along with their corresponding Pull values are:

$$C_{V_R} = 0.01 \pm 0.43i \pm (0.02 + 0.04i)\,, \quad \text{Pull} = 3.9\sigma\,, \tag{43}$$

$$C_{S_L} = -0.12 \pm 0.63i \pm (0.08 + 0.07i)\,, \quad \text{Pull} = 3.3\sigma\,. \tag{44}$$

Slightly higher Pull values are achieved when considering the complete set of observables.

3.4. LQ motivated fit scenarios

We now proceed to present the results of the fit analysis, considering additional scenarios motivated by the LQ models that we will explore in the next section. We focus exclusively on the set of HI observables specified in Eqs. (33)–(36).
The LQ models along with the combinations of Wilson coefficients not previously considered, evaluated at the LQ scale Λ_{LQ}, are:

$$S_1 : C_{V_L}, C_{S_L} = -4C_T\,, \tag{45}$$

$$U_1 : C_{V_L}, C_{S_R}\,, \tag{46}$$

$$R_2 : C_{S_L} = 4C_T\,. \tag{47}$$

Here we have the following SM quantum numbers for $R_2 = (\mathbf{3}, \mathbf{2}, 7/6)$.
After accounting for the RG running from Λ_{LQ} to μ_b, the relations $C_{S_L}(\Lambda_{LQ}) = +4C_T(\Lambda_{LQ})$ and $C_{S_L}(\Lambda_{LQ}) = -4C_T(\Lambda_{LQ})$ become respectively $C_{S_L}(\mu_b) = 8.4C_T(\mu_b)$ and $C_{S_L}(\mu_b) = -8.9C_T(\mu_b)$ [63,64]. For these two scenarios we allow Wilson coefficients to assume complex values. In this case, the best fits along with their corresponding Pull values (see Eq. (24)) are:

$$C_{S_L}(\mu_b) = 8.4C_T(\mu_b) = -0.01 \pm 0.04\,, \qquad \text{Pull} = 0.2\sigma\,, \tag{48}$$

$$C_{S_L}(\mu_b) = 8.4C_T(\mu_b) = \pm 0.53i \pm 0.05i\,, \qquad \text{Pull} = 4.2\sigma\,, \tag{49}$$

$$C_{S_L}(\mu_b) = 8.4C_T(\mu_b) = -0.07 \pm 0.55i \pm (0.04 + 0.05i)\,, \qquad \text{Pull} = 4.0\sigma\,, \tag{50}$$

$$C_{S_L}(\mu_b) = -8.9C_T(\mu_b) = 0.18 \pm 0.03\,, \qquad \text{Pull} = 4.0\sigma\,, \tag{51}$$

$$C_{S_L}(\mu_b) = -8.9C_T(\mu_b) = \pm 0.53i \pm 0.05i\,, \qquad \text{Pull} = 4.1\sigma\,, \tag{52}$$

$$C_{S_L}(\mu_b) = -8.9C_T(\mu_b) = 0.07 \pm 0.44i \pm (0.08 + 0.13i)\,, \qquad \text{Pull} = 3.8\sigma\,. \tag{53}$$

In the case where $C_{S_L}(\mu_b) = 8.4C_T(\mu_b)$, the fit indicates a clear preference for complex values. However, in general, the LQs S_1 and U_1 turn on two independent Wilson coefficients simultaneously. While the coefficients C_{V_L} and C_{S_R} are preferred to be real, we consider the two cases when the combination $C_{S_L} = -8.9C_T$ is either real or purely imaginary. We show the contour plots in Fig. 4 and Fig. 5 corresponding to the fit results:

$$S_1 : \begin{cases} C_{V_L} &= 0.09 \pm 0.04\,, \\ C_{S_L} &= -8.9C_T = -0.01 \pm 0.09\,, \end{cases} \quad \text{Pull} = 3.9\sigma \quad \rho = \begin{pmatrix} 1 & -0.93 \\ -0.93 & 1 \end{pmatrix}\,, \tag{54}$$

$$S_1 : \begin{cases} C_{V_L} &= 0.06 \pm 0.03\,, \\ C_{S_L} &= -8.9C_T = (\pm 0.34 \pm 0.13)i\,, \end{cases} \quad \text{Pull} = 4.0\sigma \quad \rho = \begin{pmatrix} 1 & 0.84 \\ 0.84 & 1 \end{pmatrix}\,, \tag{55}$$

$$U_1 : \begin{cases} C_{V_L} &= 0.07 \pm 0.02\,, \\ C_{S_R} &= 0.06 \pm 0.06\,, \end{cases} \quad \text{Pull} = 4.0\sigma \quad \rho = \begin{pmatrix} 1 & -0.77 \\ -0.77 & 1 \end{pmatrix}\,. \tag{56}$$

Differently from the case of $b \to s$ the HI observables hint to the presence of new physics in the $b \to c$ sector at four sigma level, provided future experimental analyses will avail the current results.

4. The new physics landscape

The burning question for present and future experiments in particle physics is: *Where is the scale of new physics?* This overarching goal of the present section is to answer this question by comparing time-honoured extensions of the SM, such as Z' and LQs models, with $b \to s$ and $b \to c$ observables.

4.1. Shifting up the Z' - boson

Z' bosons have a long history [65–86] and can affect FCNC, with impact for the ratios $R_{K^{(*)}}$, via their interactions

$$[g_{bs}(\bar{s}\gamma_\mu P_L b) + \text{h.c.}] + g_{\mu_L}(\bar{\mu}\gamma_\mu P_L \mu)\,, \tag{57}$$

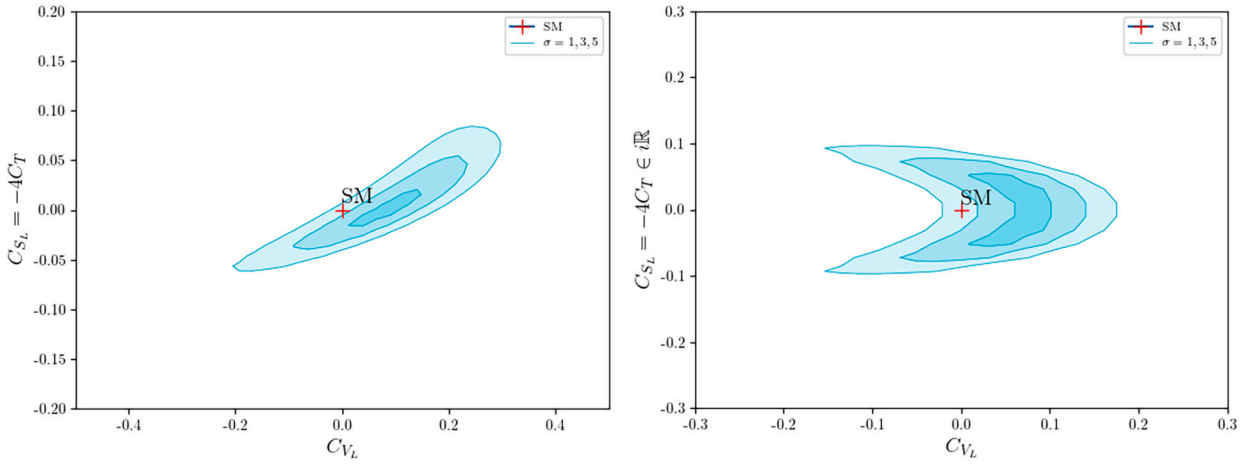

Fig. 4. Contour plots illustrating the behaviour of NP coefficients C_{V_L}, C_{S_L}, and C_T, considering the theoretical relation $C_{S_L}(\Lambda_{LQ}) = -4C_T(\Lambda_{LQ})$ predicted by the LQ S_1. The left panel represents the case where $C_{S_L} = -4C_T$ is real, while in the right panel it is purely imaginary. We present contour plots corresponding to the 1, 3, and 5-σ confidence levels, along with the corresponding SM value.

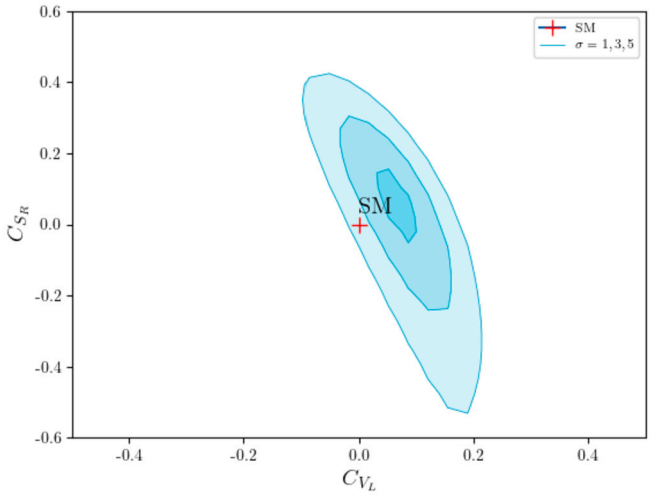

Fig. 5. Contour plot for NP coefficients C_{V_L} and C_{S_R}. We present contour plots corresponding to the 1, 3, and 5-σ confidence levels, along with the corresponding SM value.

which generates the $b \to s\ell^+\ell^-$ transitions. At tree level, a Z' with the above interactions and mass $M_{Z'}$ yields

$$C^{\text{BSM}}_{b_L\mu_L} = -\frac{4\pi v^2}{V_{tb}V^*_{ts}\alpha_{\text{em}}}\frac{g_{bs}g_{\mu_L}}{M^2_{Z'}}\,. \tag{58}$$

With the current measurements, this scenario pushes the lower bound for the Z' mass to about 50 TeV, assuming the product of the couplings to be of order unity for perturbative realizations. For this estimate we used the analytic results in (18) stemming from a direct comparison with the HI observables. We checked that if we consider the global fit with including the HS observables the result does not change.

4.2. Shrinking the leptoquarks landscape

Leptoquarks as bosonic particles carrying both quark and lepton numbers, have been extensively discussed in the literature [38, 87–105] as compelling model building especially when trying to explain possible flavor anomalies. Here we list the relevant LQs, classified by their quantum numbers under the SM gauge group $(SU(3)_c, SU(2)_L, U(1)_Y)$, and indicate for each LQ its compatibility with the up-to-date flavor data.

4.2.1. Scalar and vector leptoquarks

We consider three types of scalar LQs (S_1, R_2, S_3) and three types of vector LQs (U_1, V_2, U_3) which may still be compatible with the new picture emerging from the flavor data. We enforce baryon number conservation to prevent proton decay and further ignore couplings with right-handed neutrinos.

- $S_1 = (\bar{\mathbf{3}}, \mathbf{1}, 1/3)$

The interaction of the weak singlet scalar LQ reads:

$$y^{LL}_{1\,ij} \bar{Q}^{C\ i,a}_L S_1 (i\tau^2)^{ab} L^{j,b}_L + \ y^{RR}_{1\,ij} \bar{u}^{C\ i}_R S_1 e^j_R + \text{h.c.}\,. \tag{59}$$

The S_1 interactions can mediate at tree-level charged transitions $b \to c\tau\bar{\nu}_\tau$., with effective couplings:

$$\begin{aligned} C_{S_L} &= -4C_T = -\frac{v^2}{2V_{cb}} \frac{y^{LL}_{1\,b\tau} (y^{RR\,*}_{1\,c\tau})}{m^2_{S_1}}\ , \\ C_{V_L} &= \frac{v^2}{2V_{cb}} \frac{y^{LL}_{1\,b\tau} (V y^{LL\,*}_1)_{c\tau}}{m^2_{S_1}}\ . \end{aligned} \tag{60}$$

With these relations, S_1 can explain the observed anomalies in $R_{D^{(*)}}$. Neutral current transitions $b \to s\mu\mu$ can be also generated, but only radiatively:

$$C^{\text{BSM}}_{b_L\mu_R} = \frac{m_t^2}{8\pi\alpha_{\text{em}} m^2_{S_1}} \left(V^* y^{LL}_1\right)_{t\mu} \left(V^* y^{LL}_1\right)^*_{t\mu} - \frac{v^2}{16\pi\alpha_{\text{em}} m^2_{S_1}} \frac{\left(y^{LL}_1 \cdot y^{\dagger\,LL}_1\right)_{bs}}{V_{tb} V^*_{ts}} \left(y^{\dagger\,LL}_1 \cdot y^{LL}_1\right)_{\mu\mu}\ , \tag{61}$$

$$C^{\text{BSM}}_{b_L\mu_L} = \frac{m_t^2}{8\pi\alpha_{\text{em}} m^2_{S_1}} \left(y^{RR}_{1\,t\mu}\right) \left(y^{*\,RR}_{1\,t\mu}\right) \left[\log\left(\frac{m^2_{S_1}}{m_t^2}\right) - f(x_t)\right] - \tag{62}$$

$$- \frac{v^2}{16\pi\alpha_{\text{em}} m^2_{S_1}} \frac{\left(y^{LL}_1 \cdot y^{\dagger\,LL}_1\right)_{bs}}{V_{tb} V^*_{ts}} \left(y^{\dagger\,LL}_1 \cdot y^{LL}_1\right)_{\mu\mu}\ , \tag{63}$$

where

$$f(x_t) = 1 + \frac{3}{x_t - 1}\left(\frac{\log(x_t)}{x_t - 1} - 1\right), \quad x_t = \frac{m_t^2}{M_W^2}\ .$$

Therefore with order one couplings, we find that S_1 can explain both the $b \to c$ anomalies and the SM-like results for the $b \to s$ processes. The associated mass scale is of the order of a few TeV:

$$1.5\,\text{TeV} \lesssim m_{S_1} \lesssim 3.6\,\text{TeV}\ . \tag{64}$$

We used the analytic results for the HI observables for both type of transitions. With the upper bound coming from explaining the presence of $b \to c$ anomalies and the lower bound from not upsetting the SM-like $b \to s$ processes. If, in the future, all anomalies would disappear the upper bound will be lifted.

- $R_2 = (\mathbf{3}, \mathbf{2}, 7/6)$

R_2 is a weak doublet with interactions preserving the baryon number that are:

$$-y^{RL}_{2\,ij} \bar{u}^i_R R^a_2 (i\tau^2)^{ab} L^{j,b}_L + \ y^{LR}_{2\,ij} \bar{e}^i_R R^{a\ *}_2 Q^{j,a}_L + \text{h.c.}\,. \tag{65}$$

This model can accommodate the data on $R_{D^{(*)}}$ by generating at tree level the charged transition $b \to c\tau\bar{\nu}_\tau$, with an effective coefficient:

$$C_{S_L} = 4C_T = \frac{v^2}{2V_{cb}} \frac{y^{LR}_{2\,c\tau} (y^{RL}_{2\,b\tau})^*}{m^2_{R_2}}\ . \tag{66}$$

In fact one can generate, still at tree level, the coefficient

$$C^{\text{BSM}}_{b_L\mu_R} = -\frac{2\pi v^2}{V_{tb} V^*_{ts} \alpha_{\text{em}}} \frac{y^{LR}_{2\,s\mu} y^{LR\,*}_{2\,b\mu}}{m^2_{R_2}}\,, \tag{67}$$

relevant for the $b \to s$ processes. As a result this LQ can accommodate the $b \to c$ anomalies while agreeing with the $b \to s$ results only for specific structures of couplings such as small couplings to muons than to taus. If, however, we assume all the couplings of order one, the $b \to s$ data would require over 20 TeV for the mass of R_2 which would mean that the $b \to c$ data are not compatible with this scenario.

- $S_3 = (\bar{\mathbf{3}}, \mathbf{3}, 1/3)$
The Lagrangian of the weak triplet is given by:

$$y^L_{3\,ij} \bar{Q}^{C\ i,a}_L (i\tau^2)^{ab} \left(\tau^k S^k_3\right)^{bc} L^{j,c}_L + \text{h.c.} \tag{68}$$

Note that the couplings to diquarks are suppressed in order to guarantee proton stability. S_3 can mediate neutral current transitions $b \to s\mu\mu$ at tree-level. After integrating out the LQ, one finds

$$C^{\text{BSM}}_{b_L\mu_L} = \frac{4\pi v^2}{V_{tb}V^*_{ts}\alpha_{\text{em}}} \frac{y^L_{3\,b\mu}(y^L_{3\,s\mu})^*}{m^2_{S_3}} . \tag{69}$$

However S_3 cannot address the data $R^{exp}_{D^{(*)}} > R^{SM}_{D^{(*)}}$, since it generates a negative coefficient C_{V_L} (after accounting for the data on $B \to K^{(*)}\nu\bar{\nu}$ and Δm_{B_s}) [106]

$$C_{V_L} = -\frac{v^2}{V_{cb}} \frac{\left(V y^L_3\right)^{c\tau} y^{L\,*}_{3\,b\tau}}{m^2_{U_3}} . \tag{70}$$

Employing the constraint given in Eq. (18), we determine that the minimum threshold for the LQ scale is approximately 50 TeV.

- $U_1 = (\mathbf{3}, \mathbf{1}, 2/3)$
U_1 does not couple to diquarks and its lepto-quark interactions read:

$$x^{LL}_{1\,ij} \bar{Q}^{i,a}_L \gamma^\mu U_{1,\mu} L^{j,a}_L + x^{RR}_{1\,ij} \bar{d}^i_R \gamma^\mu U_{1,\mu} e^j_R + \text{h.c.} . \tag{71}$$

The absence of diquark interactions, and thus of proton stability issues, render this type of LQ model appealing. U_1 generates the charged transition $b \to c\tau\bar{\nu}_\tau$, with the contribution

$$\begin{aligned} C_{V_L} &= \frac{v^2}{V_{cb}} \frac{\left(V x^{LL}_1\right)_{c\tau} x^{LL\,*}_{1\,b\tau}}{m^2_{U_1}} , \\ C_{S_R} &= \frac{v^2}{2V_{cb}} \frac{\left(V x^{LL}_1\right)_{c\tau} x^{RR\,*}_{1\,b\tau}}{m^2_{U_1}} , \end{aligned} \tag{72}$$

which can accomodate $R_{D^{(*)}}$. Neglecting couplings to right-handed neutrinos, one also predicts the following Wilson's coefficients

$$\begin{aligned} C^{\text{BSM}}_{b_L\mu_L} &= -\frac{4\pi v^2}{V_{tb}V^*_{ts}\alpha_{\text{em}}} \frac{x^{LL}_{1\,s\mu} x^{LL\,*}_{1\,b\mu}}{m^2_{U_1}} , \\ C^{\text{BSM}}_{b_R\mu_R} &= -\frac{4\pi v^2}{V_{tb}V^*_{ts}\alpha_{\text{em}}} \frac{x^{RR}_{1\,s\mu} x^{RR\,*}_{1\,b\mu}}{m^2_{U_1}} . \end{aligned} \tag{73}$$

Switching on the right-handed couplings, denoted as x^{RR}_1, results in contributions to the Wilson coefficient $C^{\text{BSM}}_{b_R\mu_R}$. As mentioned in section 2.3, current $b \to s$ data disfavour this Wilson coefficient. Therefore, we set the right-handed couplings to zero $x^{RR}_1 = 0$. This scenario is referred to as the minimal U_1 model, as described in [107], where only $C^{\text{BSM}}_{b_L\mu_L}$ and C_{V_L} are turned on.

In the natural scenario where the couplings $(x^{LL}_1)^{b(c)\tau}$ and $x^{LL}_{1\,b(s)\mu}$ are all of the same order of magnitude, the constraint in Eq. (18), from HI data for the $b \to s$ sector would require over 50 TeV for the mass of U_1. However, the $b \to c$ data are not compatible with this scenario.

The LQ U_1 can accomodate both the $b \to c$ and $b \to s$ HI data under specific coupling structures, requiring a certain fine-tuning: $\frac{\left(V x^{LL}_1\right)_{c\tau} x^{LL\,*}_{1\,b\tau}}{x^{LL}_{1\,s\mu} x^{LL\,*}_{1\,b\mu}} \sim 30$.

Additionally, it is worth mentioning that the minimal U_1 scenario fails to account the recent findings from Belle II experiment concerning the branching ratio $\text{BR}(B \to K\nu\nu)$, as detailed in [108].

- $V_2 = (\mathbf{3}, \mathbf{2}, 5/6)$
The Lagrangian of the vector weak doublet V_2 is

$$x^{RL}_{2\,ij} \bar{d}^{C\ i}_R \gamma^\mu V^a_{2,\mu} (i\tau^2)^{ab} L^{j,b}_L + x^{LR}_{2\,ij} \bar{Q}^{C\ i,a}_L \gamma^\mu (i\tau^2)^{ab} V^b_{2,\mu} e^j_R + \text{h.c.} . \tag{74}$$

These interactions lead to the following contribution to the $b \to s\mu\mu$ process

$$C^{\text{BSM}}_{b_L\mu_R} = -\frac{4\pi v^2}{V_{tb}V^*_{ts}\alpha_{\text{em}}} \frac{x^{LR}_{2\,s\mu} x^{LR\,*}_{2\,b\mu}}{m^2_{V_2}} , \tag{75}$$

which is compatible with the HI data. The contribution to the $b \to c$ sector is generated at tree-level:

Table 5
Summary of leptoquark models and the relevant BSM Wilson coefficients they predict at the effective level. Checkmarks denote models successfully explaining clean observables for a particular flavor transition, while crosses signify otherwise. The final column indicates whether the model can explain both sectors simultaneously. Models marked with (✓) reproduce experimental data with small muonic coefficients.

LQ Model	Wilson Coeff.	$b \to c$	$b \to s$	$b \to c + b \to s$
S_1	$C^{\rm BSM}_{b_L\mu_L}, C^{\rm BSM}_{b_L\mu_R}, C_{V_L}, C_{S_L} = -4C_T$	✓	✓	✓
R_2	$C^{\rm BSM}_{b_L\mu_R}, C_{S_L} = 4C_T$	✓	✓	(✓)
S_3	$C^{\rm BSM}_{b_L\mu_L}, C_{V_L}$	×	✓	×
U_1	$C^{\rm BSM}_{b_L\mu_L}, C_{V_L}$	✓	✓	(✓)
V_2	$C^{\rm BSM}_{b_L\mu_R}, C_{S_R}$	✓	✓	(✓)
U_3	$C^{\rm BSM}_{b_L\mu_L}, C_{V_L}$	×	✓	×

$$C_{S_R} = -\frac{2v^2}{V_{cb}} \frac{\left(V x_2^{LR}\right)_{c\tau} x^{RL\,*}_{2\,b\tau}}{m^2_{V_2}}\,. \tag{76}$$

To describe both $b \to s$ and $b \to c$ HI data, in this case the tuning in the couplings should be: $\frac{\left(V x_2^{LR}\right)_{c\tau} x^{RL\,*}_{2\,b\tau}}{x^{LR}_{2\,s\mu} x^{LR\,*}_{2\,b\mu}} \sim 50$. If we assume all the couplings of order one, the constraint given in Eq. (19) obtained from $b \to s$ data gives a lower bound of about 30 TeV for the mass of V_2.

- $U_3 = (\mathbf{3}, \mathbf{3}, 2/3)$

The weak triplet U_3 couples only to left-handed particles via the interaction terms

$$x^{LL}_{3\,ij} \bar{Q}^{i,a}_L \gamma^\mu \left(\tau^k U^k_{3,\mu}\right)^{ab} L^{j,b}_L + \text{h.c.}\,. \tag{77}$$

As in the U_1 case, diquark couplings are absent. These interactions lead to the following contribution to the $b \to s\mu\mu$ process

$$C^{\rm BSM}_{b_L\mu_L} = -\frac{4\pi v^2}{V_{tb}V^*_{ts}\alpha_{\rm em}} \frac{x^{LL}_{3\,s\mu} x^{LL\,*}_{3\,b\mu}}{m^2_{U_3}}\,, \tag{78}$$

which affects the HI data in the $b \to s$ sector. However, it cannot explain the experimental results for the R_D and R_{D^*}, due to its negative contribution for the $b \to c\tau\bar{\nu}_\tau$ process [106]

$$C_{V_L} = -\frac{v^2}{V_{cb}} \frac{\left(V x^{LL}_3\right)^{c\tau} x^{LL\,*}_{3\,b\tau}}{m^2_{U_3}}\,. \tag{79}$$

Utilizing the constraint presented in Eq. (18), we establish that the minimum threshold for the LQ scale, required to account for the $b \to s$ HI data, is approximately 50 TeV.

We summarise our findings in Table 5: all the leptoquark models can be compatible with the SM-like results for the $b \to s$ processes. Instead, the $b \to c$ sector can be addressed by all LQ models except for the scalar S_3 and the vector U_3. Intriguingly only the S_1 state can naturally fit the overall results. For U_1, V_2 and R_2 a symmetry must be invoked protecting the couplings with muons. In the table we indicate with a (✓) the success in reproducing the experimental data conditioned to requiring new symmetry limits for the muonic coefficients.

5. Conclusions

In this work we have analysed the experimental results for the neutral and charged rare B meson decays, considering the latest measurements of the HI observables by the LHCb and CMS collaborations. We started with a theoretical investigation of the μ/e ratios R_K and R_{K^*} as well as the process $B_s \to \mu^+\mu^-$. We studied the impact of complex Wilson coefficients and derived constraints on both their imaginary and real parts. This analysis has been then followed by a comprehensive comparison with experimental results. We find that:

1. The hadronic insensitive observables are currently compatible with the Standard Model prediction within $1\,\sigma$ level.
2. When including the hadronic sensitive observables we observe that deviations from the SM persist, with a preference of new physics in the Wilson coefficient $C^{\rm BSM}_{b_L\mu_L}$ with a significance of $4.1\,\sigma$.
3. Considering simultaneously all relevant Wilson coefficients and combining both hadronic sensitive and insensitive data into the fit, the deviation from the SM is observed at $4.3\,\sigma$ and decreases at the $3.3\,\sigma$, when considering the Pull value.

Moving on to investigate the $b \to c$ anomalies, where a violation of leptonic flavor universality is still evident in the latest measurements, we performed an analysis on the complex Wilson coefficients, establishing constraints on both their imaginary and real components. Following this analysis, the comparison with experimental results reveals that:

1. Deviations from the Standard Model predictions persist, showing preference towards the emergence of a non-vanishing real-valued NP induced coefficient C_{V_L} with a significance of $4.3\,\sigma$ when solely focusing on the hadronic insensitive observables.
2. Leptoquark motivated scenarios where two Wilson coefficients are simultaneously turned on were considered, indicating a deviation at $4\,\sigma$ when employing the Pull value. This means that these models are well suited as successful extensions of the Standard Model.

Finally, we reviewed different leptoquark models aimed at explaining the deviations from the Standard Model arriving at the conclusions that: The S_1 leptoquark with a mass in the TeV range can naturally explain the SM-like $b \to s$ results and the anomalous deviation of the $b \to c$ processes. If, however, one is willing to accept unnaturally small couplings to the second generation leptons also the leptoquarks U_1, V_2 and R_2 can be employed.

Overall, even though the landscape of new physics theories has considerably shrunk some motivated extensions are still phenomenologically relevant and worth pursuing via experimental searches.

Declaration of competing interest

The authors declare that they have no known competing financial interests or personal relationships that could have appeared to influence the work reported in this paper.

Data availability

All data used are publicly available.

Acknowledgements

The work of F.S. is partially supported by the Carlsberg Foundation, semper ardens grant CF22-0922.
The work of N.V. is supported by ICSC – Centro Nazionale di Ricerca in High Performance Computing, Big Data and Quantum Computing, funded by European Union – NextGenerationEU, reference code CN 00000013.

Appendix A. Observables

In Tables 6–10 we summarise the observables used in addition to the 'hadronic insensitive' observables for both $b \to s$ and $b \to c$ sectors. All bins are treated in the experimental analyses as independent, even if overlapping.

Table 6
List of angular observables used in the global fit in addition to the 'hadronic insensitive' observables for the $b \to s$ sector. The bins highlighted in blue refer to measurements which deviate more than 2.5 σ from the theoretical prediction.

Angular observables	
Observable	$[q^2_{\text{min}}, q^2_{\text{max}}]$ [GeV^2]
LHCb $B^+ \to K^{*+}\mu\mu$ 2020 [11], $B^0 \to K^{*0}\mu\mu$ 2020 S [11]	
$\langle F_L \rangle$	[1.1, 6], [15, 19], [0.1, 0.98], [1.1, 2.5], [2.5, 4], [4, 6], [15, 17], [17, 19]
$\langle S_3 \rangle$	[1.1, 6], [15, 19], [0.1, 0.98], [1.1, 2.5], [2.5, 4], [4, 6], [15, 17], [17, 19]
$\langle S_4 \rangle$	[1.1, 6], [15, 19], [0.1, 0.98], [1.1, 2.5], [2.5, 4], [4, 6], [15, 17], [17, 19]
$\langle S_5 \rangle$	[1.1, 6], [15, 19], [0.1, 0.98], [1.1, 2.5], [2.5, 4], [4, 6], [15, 17], [17, 19]
$\langle S_7 \rangle$	[1.1, 6], [15, 19], [0.1, 0.98], [1.1, 2.5], [2.5, 4], [4, 6], [15, 17], [17, 19]
$\langle S_8 \rangle$	[1.1, 6], [15, 19], [0.1, 0.98], [1.1, 2.5], [2.5, 4], [4, 6], [15, 17], [17, 19]
$\langle S_9 \rangle$	[1.1, 6], [15, 19], [0.1, 0.98], [1.1, 2.5], [2.5, 4], [4, 6], [15, 17], [17, 19]
$\langle A_{FB} \rangle$	[1.1, 6], [15, 19], [0.1, 0.98], [1.1, 2.5], [2.5, 4], [4, 6], [15, 17], [17, 19]
$\langle P_1 \rangle$	[1.1, 6], [15, 19], [0.1, 0.98], [1.1, 2.5], [2.5, 4], [4, 6], [15, 17], [17, 19]
$\langle P_2 \rangle$	[1.1, 6], [15, 19], [0.1, 0.98], [1.1, 2.5], [2.5, 4], [4, 6], [15, 17], [17, 19]
$\langle P_3 \rangle$	[1.1, 6], [15, 19], [0.1, 0.98], [1.1, 2.5], [2.5, 4], [4, 6], [15, 17], [17, 19]
$\langle P'_4 \rangle$	[1.1, 6], [15, 19], [0.1, 0.98], [1.1, 2.5], [2.5, 4], [4, 6], [15, 17], [17, 19]
$\langle P'_5 \rangle$	[1.1, 6], [15, 19], [0.1, 0.98], [1.1, 2.5], [2.5, 4], [4, 6] , [15, 17], [17, 19]
$\langle P'_6 \rangle$	[1.1, 6], [15, 19], [0.1, 0.98], [1.1, 2.5], [2.5, 4], [4, 6], [15, 17], [17, 19]
$\langle P'_8 \rangle$	[1.1, 6], [15, 19], [0.1, 0.98], [1.1, 2.5], [2.5, 4], [4, 6], [15, 17], [17, 19]

(*continued on next page*)

Table 6 (*continued*)

Angular observables	
Observable	$[q^2_{\text{min}}, q^2_{\text{max}}]$ [GeV^2]
CMS $B \to K^* \mu\mu$ 2017 [18]	
$\langle P_1 \rangle (B^0 \to K^* \mu\mu)$	[1, 2], [2, 4.3], [4.3, 6], [16, 19]
$\langle P'_5 \rangle (B^0 \to K^* \mu\mu)$	[1, 2], [2, 4.3], [4.3, 6], [16, 19]
ATLAS $B \to K^* \mu\mu$ 2017 [19]	
$\langle F_L \rangle (B^0 \to K^* \mu\mu)$	[0.04, 2], [2, 4], [4, 6], [0.04, 4], [1.1, 6], [0.04, 6]
$\langle S_3 \rangle (B^0 \to K^* \mu\mu)$	[0.04, 2], [2, 4], [4, 6], [0.04, 4], [1.1, 6], [0.04, 6]
$\langle S_4 \rangle (B^0 \to K^* \mu\mu)$	[0.04, 2], [2, 4], [4, 6], [0.04, 4], [1.1, 6], [0.04, 6]
$\langle S_5 \rangle (B^0 \to K^* \mu\mu)$	[0.04, 2], [2, 4], [4, 6], [0.04, 4], [1.1, 6], [0.04, 6]
$\langle S_7 \rangle (B^0 \to K^* \mu\mu)$	[0.04, 2], [2, 4], [4, 6], [0.04, 4], [1.1, 6], [0.04, 6]
$\langle S_8 \rangle (B^0 \to K^* \mu\mu)$	[0.04, 2], [2, 4], [4, 6], [0.04, 4], [1.1, 6], [0.04, 6]
$\langle P_1 \rangle (B^0 \to K^* \mu\mu)$	[0.04, 2], [2, 4], [4, 6], [0.04, 4], [1.1, 6], [0.04, 6]
$\langle P'_4 \rangle (B^0 \to K^* \mu\mu)$	[0.04, 2], [2, 4], [4, 6], [0.04, 4], [1.1, 6], [0.04, 6]
$\langle P'_5 \rangle (B^0 \to K^* \mu\mu)$	[0.04, 2], [2, 4], [4, 6], [0.04, 4], [1.1, 6], [0.04, 6]
$\langle P'_6 \rangle (B^0 \to K^* \mu\mu)$	[0.04, 2], [2, 4], [4, 6], [0.04, 4], [1.1, 6], [0.04, 6]
$\langle P'_8 \rangle (B^0 \to K^* \mu\mu)$	[0.04, 2], [2, 4], [4, 6], [0.04, 4], [1.1, 6], [0.04, 6]

Table 7
List of differential branching ratios used in the global fit in addition to the 'hadronic insensitive' observables for the $b \to s$ sector. The bins highlighted in blue and red indicate measurements which deviate more than 2.5 and 3.5 σ from the theoretical prediction, respectively.

Branching ratios	
Observable	$[q^2_{\text{min}}, q^2_{\text{max}}]$ [GeV^2]
LHCb $B^\pm \to K \mu\mu$ 2014 [5]	
$\frac{d}{dq^2}\text{BR}(B^\pm \to K \mu\mu)$	[0.1, 0.98], [1.1, 2], [2, 3], [3, 4], [4, 5], [5, 6], [15, 16], [16, 17], [17, 18], [18, 19], [19, 20], [20, 21], [21, 22], [1.1, 6], [15, 22]
LHCb $B^0 \to K \mu\mu$ 2014 [5]	
$\frac{d}{dq^2}\text{BR}(B^0 \to K \mu\mu)$	[0.1, 2], [2, 4], [4, 6], [15, 17], [17, 22], [1.1, 6], [15, 22]
LHCb $B^\pm \to K^* \mu\mu$ 2014 [5]	
$\frac{d}{dq^2}\text{BR}(B^\pm \to K^* \mu\mu)$	[0.1, 2], [2, 4], [4, 6], [15, 17], [17, 19], [1.1, 6], [15, 19]
LHCb $B^0 \to K^* \mu\mu$ 2016 [15]	
$\frac{d}{dq^2}\text{BR}(B^0 \to K^* \mu\mu)$	[0.1, 0.98], [1.1, 2.5], [2.5, 4], [4, 6], [15, 17], [17, 19], [1.1, 6], [15, 19]
LHCb $B_s \to \phi \mu\mu$ 2021 [10]	
$\frac{d}{dq^2}\text{BR}(B_s \to \phi \mu\mu)$	[0.1, 0.98], [1.1, 2.5], [2.5, 4], [4, 6], [15, 17], [17, 19], [1.1, 6], [15, 19]
Babar $B \to X_s ll$ 2013 [16]	
$\frac{d}{dq^2}\text{BR}(B \to X_s ll)$	[0.1, 2], [2.0, 4.3], [4.3, 6.8], [1, 6], [14,2, 25]
$\frac{d}{dq^2}\text{BR}(B \to X_s \mu\mu)$	[0.1, 2], [2.0, 4.3], [4.3, 6.8], [1, 6], [14,2, 25]
$\frac{d}{dq^2}\text{BR}(B \to X_s ee)$	[0.1, 2], [2.0, 4.3], [4.3, 6.8], [1, 6], [14,2, 25]
Belle $B \to X_s ll$ 2005 [17]	
$\frac{d}{dq^2}\text{BR}(B \to X_s ll)$	[0.04, 1], [1, 6], [14.4, 25]

Table 8
List of branching ratios within the different q^2-bins employed in the global fit for the $b \to c$ sector.

Binned Branching ratios	
Observable	$[q^2_{\min}, q^2_{\max}]$ [GeV^2]
Belle $B^+ \to D\mu\nu_\mu$ 2015 [109]	
BR($B^+ \to D\mu\nu_\mu$)	[0.0, 1.03], [1.03, 2.21], [2.21, 3.39], [3.39, 4.57], [4.57, 5.75], [5.75, 6.93], [6.93, 8.11], [8.11, 9.3], [9.3, 10.48], [10.48, 11.66]
Belle $B^0 \to D\mu\nu_\mu$ 2015 [109]	
BR($B^0 \to D\mu\nu_\mu$)	[0.0, 1.03], [1.03, 2.21], [2.21, 3.39], [3.39, 4.57], [4.57, 5.75], [5.75, 6.93],[6.93, 8.11], [8.11, 9.3], [9.3, 10.48], [10.48, 11.66]
Belle $B^+ \to De\nu_e$ 2015 [109]	
BR($B^+ \to De\nu_e$)	[0.0, 1.03], [1.03, 2.21], [2.21, 3.39], [3.39, 4.57], [4.57, 5.75], [5.75, 6.93],[6.93, 8.11], [8.11, 9.3], [9.3, 10.48], [10.48, 11.66]
Belle $B^0 \to De\nu_e$ 2015 [109]	
BR($B^0 \to De\nu_e$)	[0.0, 1.03], [1.03, 2.21], [2.21, 3.39], [3.39, 4.57], [4.57, 5.75], [5.75, 6.93],[6.93, 8.11], [8.11, 9.3], [9.3, 10.48], [10.48, 11.66]
Babar $B^+ \to D\ell\nu_\ell$ 2009 [110]	
BR($B^+ \to D\ell\nu_\ell$)	[0.0, 0.97], [0.97, 2.15], [2.15, 3.34], [3.34, 4.52], [4.52, 5.71], [5.71, 6.89], [6.89, 8.07], [8.07, 9.26], [9.26, 10.44], [10.44, 11.63]
Belle $B \to D^*\mu\nu_\mu$ 2010 [111]	
BR$_L$($B \to D^*\mu\nu_\mu$)	[0.08, 1.14], [1.14, 2.2], [2.2, 3.26], [3.26, 4.32], [4.32, 5.38], [5.38, 6.44], [6.44, 7.5], [7.5, 8.57], [8.57, 9.63], [9.63, 10.69]
BR$_T$($B \to D^*\mu\nu_\mu$)	[0.08, 1.14], [1.14, 2.2], [2.2, 3.26], [3.26, 4.32], [4.32, 5.38], [5.38, 6.44], [6.44, 7.5], [7.5, 8.57], [8.57, 9.63], [9.63, 10.69]
Belle $B \to D^*e\nu_e$ 2010 [111]	
BR$_L$($B \to D^*e\nu_e$)	[0.08, 1.14], [1.14, 2.2], [2.2, 3.26], [3.26, 4.32], [4.32, 5.38], [5.38, 6.44], [6.44, 7.5], [7.5, 8.57], [8.57, 9.63], [9.63, 10.69]
BR$_T$($B \to D^*e\nu_e$)	[0.08, 1.14], [1.14, 2.2], [2.2, 3.26], [3.26, 4.32], [4.32, 5.38], [5.38, 6.44], [6.44, 7.5], [7.5, 8.57], [8.57, 9.63], [9.63, 10.69]
Belle $B^0 \to D^*\ell\nu_\ell$ 2017 [112]	
BR($B^0 \to D^*\ell\nu_\ell$)	[0.0, 1.14], [1.14, 2.2], [2.2, 3.26], [3.26, 4.32], [4.32, 5.38], [5.38, 6.44], [6.44, 7.5], [7.5, 8.57], [8.57, 9.63], [9.63, 10.69]

Table 9
List of branching ratios within the different bins employed in the global fit for the $b \to c$ sector.

Binned Branching ratios	
Observable	$[\cos\theta_v^{\min}, \cos\theta_v^{\max}]$ [112]
BR($B \to D^*\ell\nu_\ell$)	[-1.0, -0.8], [-0.8,-0.6],[-0.6,-0.4], [-0.4,-0.2],[-0.2,0.0], [0.2,0.4] ,[0.4,0.6],[0.6,0.8], [0.8,1.0]
$[\cos\theta_l^{\min}, \cos\theta_l^{\max}]$ [112]	
BR($B \to D^*\ell\nu_\ell$)	[-1.0, -0.8], [-0.8,-0.6],[-0.6,-0.4], [-0.4,-0.2],[-0.2,0.0], [0.2,0.4],[0.4,0.6],[0.6,0.8], [0.8,1.0]
$[\phi^{\min}, \phi^{\max}]$ [112]	
BR($B \to D^*\ell\nu_\ell$)	$[0.0, \pi/5], [\pi/5, 2\pi/5], [2\pi/5, 3\pi/5], [3\pi/5, 4\pi/5], [4\pi/5, \pi]$, $[\pi, 6\pi/5], [6\pi/5, 7\pi/5], [7\pi/5, 8\pi/5], [8\pi/5, 9\pi/5], [9\pi/5, 2\pi]$

Table 10
List of total branching ratios used in the global fit for the $b \to c$ sector.

Total Branching ratios [113–118]	
Observable	BR($B^+ \to De\nu_e$), BR($B^+ \to D^*e\nu_e$) , BR($B^+ \to D\mu\nu_\mu$) BR($B^+ \to D^*\mu\nu_\mu$) , BR($B^+ \to D^*\ell\nu_\ell$) , BR($B^0 \to D^*\ell\nu_\ell$)

References

[1] Alessandra D'Alise, et al., Standard model anomalies: lepton flavour non-universality, g – 2 and W-mass, J. High Energy Phys. 08 (2022) 125, https://doi.org/10.1007/JHEP08(2022)125, arXiv:2204.03686 [hep-ph].

[2] R. Aaij, et al., Test of lepton universality in $b \to s\ell^+\ell^-$ decays, Phys. Rev. Lett. 131 (5) (2023) 051803, https://doi.org/10.1103/PhysRevLett.131.051803, arXiv:2212.09152 [hep-ex].

[3] R. Aaij, et al., Measurement of lepton universality parameters in $B^+ \to K^+\ell^+\ell^-$ and $B^0 \to K^{*0}\ell^+\ell^-$ decays, Phys. Rev. D 108 (3) (2023) 032002, https://doi.org/10.1103/PhysRevD.108.032002, arXiv:2212.09153 [hep-ex].

[4] Yasmine Sara Amhis, et al., Averages of b-hadron, c-hadron, and τ-lepton properties as of 2021, Phys. Rev. D 107 (5) (2023) 052008, https://doi.org/10.1103/PhysRevD.107.052008, arXiv:2206.07501 [hep-ex].

[5] R. Aaij, et al., Differential branching fractions and isospin asymmetries of $B \to K^{(*)}\mu^+\mu^-$ decays, J. High Energy Phys. 06 (2014) 133, https://doi.org/10.1007/JHEP06(2014)133, arXiv:1403.8044 [hep-ex].

[6] S. Choudhury, et al., Test of lepton flavor universality and search for lepton flavor violation in $B \to K\ell\ell$ decays, J. High Energy Phys. 03 (2021) 105, https://doi.org/10.1007/JHEP03(2021)105, arXiv:1908.01848 [hep-ex].

[7] R. Aaij, et al., Test of lepton universality with $B^0 \to K^{*0}\ell^+\ell^-$ decays, J. High Energy Phys. 08 (2017) 055, https://doi.org/10.1007/JHEP08(2017)055, arXiv:1705.05802 [hep-ex].

[8] Roel Aaij, et al., Test of lepton universality in beauty-quark decays, Nat. Phys. 18 (3) (2022) 277–282, Addendum: Nat. Phys. 19 (2023), https://doi.org/10.1038/s41567-023-02095-3, arXiv:2103.11769.

[9] Roel Aaij, et al., Measurement of the $B_s^0 \to \mu^+\mu^-$ decay properties and search for the $B^0 \to \mu^+\mu^-$ and $B_s^0 \to \mu^+\mu^-\gamma$ decays, Phys. Rev. D 105 (1) (2022) 012010, https://doi.org/10.1103/PhysRevD.105.012010, arXiv:2108.09283 [hep-ex].

[10] Roel Aaij, et al., Branching fraction measurements of the rare $B_s^0 \to \phi\mu^+\mu^-$ and $B_s^0 \to f_2'(1525)\mu^+\mu^-$ decays, Phys. Rev. Lett. 127 (15) (2021) 151801, https://doi.org/10.1103/PhysRevLett.127.151801, arXiv:2105.14007 [hep-ex].

[11] Roel Aaij, et al., Angular analysis of the $B^+ \to K^{*+}\mu^+\mu^-$ decay, Phys. Rev. Lett. 126 (16) (2021) 161802, https://doi.org/10.1103/PhysRevLett.126.161802, arXiv:2012.13241 [hep-ex].

[12] A. Abdesselam, et al., Test of lepton-flavor universality in $B \to K^*\ell^+\ell^-$ decays at Belle, Phys. Rev. Lett. 126 (16) (2021) 161801, https://doi.org/10.1103/PhysRevLett.126.161801, arXiv:1904.02440 [hep-ex].

[13] Aaboud Morad, et al., Study of the rare decays of B_s^0 and B^0 mesons into muon pairs using data collected during 2015 and 2016 with the ATLAS detector, J. High Energy Phys. 04 (2019) 098, https://doi.org/10.1007/JHEP04(2019)098, arXiv:1812.03017 [hep-ex].

[14] CMS Collaboration, Measurement of properties of Bs0 to mu+mu- decays and search for B0 to mu+mu- with the CMS experiment, 2019.

[15] Roel Aaij, et al., Measurements of the s-wave fraction in $B^0 \to K^+\pi^-\mu^+\mu^-$ decays and the $B^0 \to K^*(892)^0\mu^+\mu^-$ differential branching fraction, J. High Energy Phys. 11 (2016) 047, Erratum: J. High Energy Phys. 04 (2017) 142, https://doi.org/10.1007/JHEP11(2016)047, arXiv:1606.04731 [hep-ex].

[16] J.P. Lees, et al., Measurement of the $B \to X_s l^+ l^-$ branching fraction and search for direct CP violation from a sum of exclusive final states, Phys. Rev. Lett. 112 (2014) 211802, https://doi.org/10.1103/PhysRevLett.112.211802, arXiv:1312.5364 [hep-ex].

[17] M. Iwasaki, et al., Improved measurement of the electroweak penguin process $B \to X_s l^+ l^-$, Phys. Rev. D 72 (2005) 092005, https://doi.org/10.1103/PhysRevD.72.092005, arXiv:hep-ex/0503044.

[18] Measurement of the P_1 and P_5' angular parameters of the decay $B^0 \to K^{*0}\mu^+\mu^-$ in proton-proton collisions at $\sqrt{s} = 8$ TeV, 2017, https://doi.org/10.1016/j.physletb.2018.04.030.

[19] Angular analysis of $B_d^0 \to K^*\mu^+\mu^-$ decays in pp collisions at $\sqrt{s} = 8$ TeV with the ATLAS detector. Ed. by Etienne Auge, Jacques Dumarchez, Jean Tran Thanh Van. Apr. 2017, https://doi.org/10.1007/JHEP10(2018)047.

[20] David M. Straub, Flavio: a Python package for flavour and precision phenomenology in the Standard Model and beyond, arXiv:1810.08132 [hep-ph], Oct. 2018.

[21] Jason Aebischer, Matteo Fael, Christoph Greub, Javier Virto, B physics beyond the standard model at one loop: complete renormalization group evolution below the electroweak scale, J. High Energy Phys. 09 (2017) 158, https://doi.org/10.1007/JHEP09(2017)158, arXiv:1704.06639 [hep-ph].

[22] Jason Aebischer, Jacky Kumar, David M. Straub, Wilson: a Python package for the running and matching of Wilson coefficients above and below the electroweak scale, Eur. Phys. J. C 78 (12) (2018) 1026, https://doi.org/10.1140/epjc/s10052-018-6492-7, arXiv:1804.05033 [hep-ph].

[23] Rodrigo Alonso, Benjamin Grinstein, Jorge Martin Camalich, $SU(2) \times U(1)$ gauge invariance and the shape of new physics in rare B decays, Phys. Rev. Lett. 113 (2014) 241802, https://doi.org/10.1103/PhysRevLett.113.241802, arXiv:1407.7044 [hep-ph].

[24] Gudrun Hiller, Frank Kruger, More model-independent analysis of $b \to s$ processes, Phys. Rev. D 69 (2004) 074020, https://doi.org/10.1103/PhysRevD.69.074020, arXiv:hep-ph/0310219.

[25] Guido D'Amico, Marco Nardecchia, Paolo Panci, Francesco Sannino, Alessandro Strumia, Riccardo Torre, Alfredo Urbano, Flavour anomalies after the R_{K^*} measurement, J. High Energy Phys. 09 (2017) 010, https://doi.org/10.1007/JHEP09(2017)010, arXiv:1704.05438 [hep-ph].

[26] Christoph Bobeth, Gudrun Hiller, Giorgi Piranishvili, CP asymmetries in bar $B \to \bar{K}(\to \bar{K}\pi)\bar{\ell}\ell$ and untagged $\bar{B}_s$, $B_s \to \phi(\to K^+K^-)\bar{\ell}\ell$ decays at NLO, J. High Energy Phys. 07 (2008) 106, https://doi.org/10.1088/1126-6708/2008/07/106, arXiv:0805.2525 [hep-ph].

[27] Christian Hambrock, Gudrun Hiller, Stefan Schacht, Roman Zwicky, $B \to K^\star$ form factors from flavor data to QCD and back, Phys. Rev. D 89 (7) (2014) 074014, https://doi.org/10.1103/PhysRevD.89.074014, arXiv:1308.4379 [hep-ph].

[28] Gudrun Hiller, Martin Schmaltz, Diagnosing lepton-nonuniversality in $b \to s\ell\ell$, J. High Energy Phys. 02 (2015) 055, https://doi.org/10.1007/JHEP02(2015)055, arXiv:1411.4773 [hep-ph].

[29] Neetu Raj Singh Chundawat, New physics in B→K*$\tau+\tau-$: a model independent analysis, Phys. Rev. D 107 (5) (2023) 055004, https://doi.org/10.1103/PhysRevD.107.055004, arXiv:2212.01229 [hep-ph].

[30] Neetu Raj Singh Chundawat, CP violation in $b \to s\ell\ell$: a model independent analysis, Phys. Rev. D 107 (2023) 075014, https://doi.org/10.1103/PhysRevD.107.075014, arXiv:2207.10613 [hep-ph].

[31] Armen Tumasyan, et al., Measurement of the $B_S^0 \to \mu^+\mu^-$ decay properties and search for the $B^0 \to \mu^+\mu^-$ decay in proton-proton collisions at $\sqrt{s} = 13$ TeV, Phys. Lett. B 842 (2023) 137955, https://doi.org/10.1016/j.physletb.2023.137955, arXiv:2212.10311 [hep-ex].

[32] Allanach Ben, Joe Davighi, The Rumble in the Meson: a leptoquark versus a Z' to fit b → s$\mu^+\mu^-$ anomalies including 2022 LHCb $R_{K^{(*)}}$ measurements, J. High Energy Phys. 04 (2023) 033, https://doi.org/10.1007/JHEP04(2023)033, arXiv:2211.11766 [hep-ph].

[33] Diptimoy Ghosh, Marco Nardecchia, S.A. Renner, Hint of lepton flavour non-universality in B meson decays, J. High Energy Phys. 12 (2014) 131, https://doi.org/10.1007/JHEP12(2014)131, arXiv:1408.4097 [hep-ph].

[34] Wolfgang Altmannshofer, David M. Straub, New physics in $b \to s$ transitions after LHC run 1, Eur. Phys. J. C 75 (8) (2015) 382, https://doi.org/10.1140/epjc/s10052-015-3602-7, arXiv:1411.3161 [hep-ph].

[35] Sébastien Descotes-Genon, Lars Hofer, Joaquim Matias, Javier Virto, Global analysis of $b \to s\ell\ell$ anomalies, J. High Energy Phys. 06 (2016) 092, https://doi.org/10.1007/JHEP06(2016)092, arXiv:1510.04239 [hep-ph].

[36] Wolfgang Altmannshofer, David M. Straub, New physics in $B \to K^*\mu\mu$?, Eur. Phys. J. C 73 (2013) 2646, https://doi.org/10.1140/epjc/s10052-013-2646-9, arXiv:1308.1501 [hep-ph].

[37] Tobias Hurth, Farvah Mahmoudi, On the LHCb anomaly in B → $K^*\ell^+\ell^-$, J. High Energy Phys. 04 (2014) 097, https://doi.org/10.1007/JHEP04(2014)097, arXiv:1312.5267 [hep-ph].

[38] Gudrun Hiller, Martin Schmaltz, R_K and future $b \to s\ell\ell$ physics beyond the standard model opportunities, Phys. Rev. D 90 (2014) 054014, https://doi.org/10.1103/PhysRevD.90.054014, arXiv:1408.1627 [hep-ph].

[39] T. Hurth, F. Mahmoudi, S. Neshatpour, Global fits to $b \to s\ell\ell$ data and signs for lepton non-universality, J. High Energy Phys. 12 (2014) 053, https://doi.org/10.1007/JHEP12(2014)053, arXiv:1410.4545 [hep-ph].

[40] Marco Ciuchini, Antonio M. Coutinho, Marco Fedele, Enrico Franco, Ayan Paul, Luca Silvestrini, Mauro Valli, On flavourful easter eggs for new physics hunger and lepton flavour universality violation, Eur. Phys. J. C 77 (10) (2017) 688, https://doi.org/10.1140/epjc/s10052-017-5270-2, arXiv:1704.05447 [hep-ph].

[41] Bernat Capdevila, Andreas Crivellin, Sébastien Descotes-Genon, Joaquim Matias, Javier Virto, Patterns of new physics in $b \to s\ell^+\ell^-$ transitions in the light of recent data, J. High Energy Phys. 01 (2018) 093, https://doi.org/10.1007/JHEP01(2018)093, arXiv:1704.05340 [hep-ph].

[42] Wolfgang Altmannshofer, Christoph Niehoff, Peter Stangl, David M. Straub, Status of the $B \to K^*\mu^+\mu^-$ anomaly after Moriond 2017, Eur. Phys. J. C 77 (6) (2017) 377, https://doi.org/10.1140/epjc/s10052-017-4952-0, arXiv:1703.09189 [hep-ph].

[43] Marcel Algueró, Bernat Capdevila, Andreas Crivellin, Sébastien Descotes-Genon, Pere Masjuan, Joaquim Matias, Martín Novoa Brunet, Javier Virto, Emerging patterns of new physics with and without lepton flavour universal contributions, Eur. Phys. J. C 79 (8) (2019) 714, Addendum: Eur. Phys. J. C 80 (511) (2020), https://doi.org/10.1140/epjc/s10052-019-7216-3, arXiv:1903.09578 [hep-ph].

[44] Jason Aebischer, Wolfgang Altmannshofer, Diego Guadagnoli, Méril Reboud, Peter Stangl, David M. Straub, B-decay discrepancies after Moriond 2019, Eur. Phys. J. C 80 (3) (2020) 252, https://doi.org/10.1140/epjc/s10052-020-7817-x, arXiv:1903.10434 [hep-ph].

[45] Marco Ciuchini, Marco Fedele, Enrico Franco, Ayan Paul, Luca Silvestrini, Mauro Valli, Lessons from the $B^{0,+} \to K^{*0,+}\mu^+\mu^-$ angular analyses, Phys. Rev. D 103 (1) (2021) 015030, https://doi.org/10.1103/PhysRevD.103.015030, arXiv:2011.01212 [hep-ph].

[46] Monika Blanke, Andreas Crivellin, Stefan de Boer, Teppei Kitahara, Marta Moscati, Ulrich Nierste, Ivan Nišandžić, Impact of polarization observables and $B_c \to \tau\nu$ on new physics explanations of the $b \to c\tau\nu$ anomaly, Phys. Rev. D 99 (7) (2019) 075006, https://doi.org/10.1103/PhysRevD.99.075006, arXiv:1811.09603 [hep-ph].

[47] Admir Greljo, Dean J. Robinson, Bibhushan Shakya, Jure Zupan, R(D$^{(*)}$) from W′ and right-handed neutrinos, J. High Energy Phys. 09 (2018) 169, https://doi.org/10.1007/JHEP09(2018)169, arXiv:1804.04642 [hep-ph].

[48] Pouya Asadi, Matthew R. Buckley, David Shih, It's all right(-handed neutrinos): a new W′ model for the $R_{D^{(*)}}$ anomaly, J. High Energy Phys. 09 (2018) 010, https://doi.org/10.1007/JHEP09(2018)010, arXiv:1804.04135 [hep-ph].

[49] Dean J. Robinson, Bibhushan Shakya, Jure Zupan, Right-handed neutrinos and R(D$^{(*)}$), J. High Energy Phys. 02 (2019) 119, https://doi.org/10.1007/JHEP02(2019)119, arXiv:1807.04753 [hep-ph].

[50] A. Author, Title of the talk. Belle2 collaboration talk, https://docs.belle2.org/record/3746/files/BELLE2-TALK-CONF-2023-097.pdf?version=2, 2023.

[51] Rodrigo Alonso, Benjamín Grinstein, Jorge Martin Camalich, Lifetime of B_c^- constrains explanations for anomalies in $B \to D^{(*)}\tau\nu$, Phys. Rev. Lett. 118 (8) (2017) 081802, https://doi.org/10.1103/PhysRevLett.118.081802, arXiv:1611.06676 [hep-ph].

[52] A.G. Akeroyd, Chuan-Hung Chen, Constraint on the branching ratio of $B_c \to \tau\bar{\nu}$ from LEP1 and consequences for $R(D^{(*)})$ anomaly, Phys. Rev. D 96 (7) (2017) 075011, https://doi.org/10.1103/PhysRevD.96.075011, arXiv:1708.04072 [hep-ph].

[53] A. Abdesselam, et al., Measurement of the D^{*-} polarization in the decay $B^0 \to D^{*-}\tau^+\nu_\tau$, in: 10th International Workshop on the CKM Unitarity Triangle, Mar. 2019, arXiv:1903.03102 [hep-ex].

[54] J.P. Lees, et al., Evidence for an excess of $\bar{B} \to D^{(*)}\tau^-\bar{\nu}_\tau$ decays, Phys. Rev. Lett. 109 (2012) 101802, https://doi.org/10.1103/PhysRevLett.109.101802, arXiv:1205.5442 [hep-ex].

[55] J.P. Lees, et al., Measurement of an excess of $\bar{B} \to D^{(*)}\tau^-\bar{\nu}_\tau$ decays and implications for charged Higgs bosons, Phys. Rev. D 88 (7) (2013) 072012, https://doi.org/10.1103/PhysRevD.88.072012, arXiv:1303.0571 [hep-ex].

[56] M. Huschle, et al., Measurement of the branching ratio of $\bar{B} \to D^{(*)}\tau^-\bar{\nu}_\tau$ relative to $\bar{B} \to D^{(*)}\ell^-\bar{\nu}_\ell$ decays with hadronic tagging at Belle, Phys. Rev. D 92 (7) (2015) 072014, https://doi.org/10.1103/PhysRevD.92.072014, arXiv:1507.03233 [hep-ex].

[57] S. Hirose, et al., Measurement of the τ lepton polarization and $R(D^*)$ in the decay $\bar{B} \to D^*\tau^-\bar{\nu}_\tau$, Phys. Rev. Lett. 118 (21) (2017) 211801, https://doi.org/10.1103/PhysRevLett.118.211801, arXiv:1612.00529 [hep-ex].

[58] S. Hirose, et al., Measurement of the τ lepton polarization and $R(D^*)$ in the decay $\bar{B} \to D^*\tau^-\bar{\nu}_\tau$ with one-prong hadronic τ decays at Belle, Phys. Rev. D 97 (1) (2018) 012004, https://doi.org/10.1103/PhysRevD.97.012004, arXiv:1709.00129 [hep-ex].

[59] A. Abdesselam, et al., Measurement of $\mathcal{R}(D)$ and $\mathcal{R}(D^*)$ with a semileptonic tagging method, arXiv:1904.08794 [hep-ex], Apr. 2019.

[60] G. Caria, et al., Measurement of $\mathcal{R}(D)$ and $\mathcal{R}(D^*)$ with a semileptonic tagging method, Phys. Rev. Lett. 124 (16) (2020) 161803, https://doi.org/10.1103/PhysRevLett.124.161803, arXiv:1910.05864 [hep-ex].

[61] Measurement of the Ratios of Branching Fractions $\mathcal{R}(D^*)$ and $\mathcal{R}(D^0)$, Phys. Rev. Lett. 131 (2023) 111802, https://doi.org/10.1103/PhysRevLett.131.111802, arXiv:2302.02886 [hep-ex].

[62] Roel Aaij, et al., Test of lepton flavor universality using B0→D*-τ+ ντ decays with hadronic τ channels, Phys. Rev. D 108 (1) (2023) 012018, https://doi.org/10.1103/PhysRevD.108.012018, arXiv:2305.01463 [hep-ex].

[63] Syuhei Iguro, Teppei Kitahara, Ryoutaro Watanabe, Global fit to $b \to c\tau\nu$ anomalies 2022 mid-autumn, arXiv:2210.10751 [hep-ph], Oct. 2022.

[64] Bernat Capdevila, Andreas Crivellin, Joaquim Matias, Review of semileptonic B anomalies, Eur. Phys. J. Spec. Top. 1 (2023) 20, https://doi.org/10.1140/epjs/s11734-023-01012-2, arXiv:2309.01311 [hep-ph].

[65] Rhorry Gauld, Florian Goertz, Ulrich Haisch, An explicit Z'-boson explanation of the $B \to K^*\mu^+\mu^-$ anomaly, J. High Energy Phys. 01 (2014) 069, https://doi.org/10.1007/JHEP01(2014)069, arXiv:1310.1082 [hep-ph].

[66] Andrzej J. Buras, Fulvia De Fazio, Jennifer Girrbach, 331 models facing new $b \to s\mu^+\mu^-$ data, J. High Energy Phys. 02 (2014) 112, https://doi.org/10.1007/JHEP02(2014)112, arXiv:1311.6729 [hep-ph].

[67] Wolfgang Altmannshofer, Stefania Gori, Maxim Pospelov, Itay Yavin, Quark flavor transitions in $L_\mu - L_\tau$ models, Phys. Rev. D 89 (2014) 095033, https://doi.org/10.1103/PhysRevD.89.095033, arXiv:1403.1269 [hep-ph].

[68] Andreas Crivellin, Giancarlo D'Ambrosio, Julian Heeck, Explaining $h \to \mu^\pm\tau^\mp$, $B \to K^*\mu^+\mu^-$ and $B \to K\mu^+\mu^-/B \to Ke^+e^-$ in a two-Higgs-doublet model with gauged $L_\mu - L_\tau$, Phys. Rev. Lett. 114 (2015) 151801, https://doi.org/10.1103/PhysRevLett.114.151801, arXiv:1501.00993 [hep-ph].

[69] Andreas Crivellin, Giancarlo D'Ambrosio, Julian Heeck, Addressing the LHC flavor anomalies with horizontal gauge symmetries, Phys. Rev. D 91 (7) (2015) 075006, https://doi.org/10.1103/PhysRevD.91.075006, arXiv:1503.03477 [hep-ph].

[70] Christoph Niehoff, Peter Stangl, David M. Straub, Violation of lepton flavour universality in composite Higgs models, Phys. Lett. B 747 (2015) 182–186, https://doi.org/10.1016/j.physletb.2015.05.063, arXiv:1503.03865 [hep-ph].

[71] Alejandro Celis, Javier Fuentes-Martin, Martin Jung, Hugo Serodio, Family nonuniversal Z' models with protected flavor-changing interactions, Phys. Rev. D 92 (1) (2015) 015007, https://doi.org/10.1103/PhysRevD.92.015007, arXiv:1505.03079 [hep-ph].

[72] Admir Greljo, Gino Isidori, David Marzocca, On the breaking of lepton flavor universality in B decays, J. High Energy Phys. 07 (2015) 142, https://doi.org/10.1007/JHEP07(2015)142, arXiv:1506.01705 [hep-ph].

[73] Wolfgang Altmannshofer, Itay Yavin, Predictions for lepton flavor universality violation in rare b decays in models with gauged $L_\mu - L_\tau$, Phys. Rev. D 92 (7) (2015) 075022, https://doi.org/10.1103/PhysRevD.92.075022, arXiv:1508.07009 [hep-ph].

[74] Adam Falkowski, Marco Nardecchia, Robert Ziegler, Lepton flavor non-universality in B-meson decays from a U(2) flavor model, J. High Energy Phys. 11 (2015) 173, https://doi.org/10.1007/JHEP11(2015)173, arXiv:1509.01249 [hep-ph].

[75] Adrian Carmona, Florian Goertz, Lepton flavor and nonuniversality from minimal composite Higgs setups, Phys. Rev. Lett. 116 (25) (2016) 251801, https://doi.org/10.1103/PhysRevLett.116.251801, arXiv:1510.07658 [hep-ph].

[76] Florian Goertz, Jernej F. Kamenik, Andrey Katz, Marco Nardecchia, Indirect constraints on the scalar di-photon resonance at the LHC, J. High Energy Phys. 05 (2016) 187, https://doi.org/10.1007/JHEP05(2016)187, arXiv:1512.08500 [hep-ph].

[77] Cheng-Wei Chiang, Xiao-Gang He, German Valencia, Z' model for $b \to s \ell \overline{\ell}$ flavor anomalies, Phys. Rev. D 93 (7) (2016) 074003, https://doi.org/10.1103/PhysRevD.93.074003, arXiv:1601.07328 [hep-ph].

[78] Damir Bečirević, Olcyr Sumensari, Renata Zukanovich Funchal, Lepton flavor violation in exclusive $b \to s$ decays, Eur. Phys. J. C 76 (3) (2016) 134, https://doi.org/10.1140/epjc/s10052-016-3985-0, arXiv:1602.00881 [hep-ph].

[79] Sofiane M. Boucenna, Alejandro Celis, Javier Fuentes-Martin, Avelino Vicente, Javier Virto, Non-abelian gauge extensions for B-decay anomalies, Phys. Lett. B 760 (2016) 214–219, https://doi.org/10.1016/j.physletb.2016.06.067, arXiv:1604.03088 [hep-ph].

[80] Sofiane M. Boucenna, Alejandro Celis, Javier Fuentes-Martin, Avelino Vicente, Javier Virto, Phenomenology of an $SU(2) \times SU(2) \times U(1)$ model with lepton-flavour non-universality, J. High Energy Phys. 12 (2016) 059, https://doi.org/10.1007/JHEP12(2016)059, arXiv:1608.01349 [hep-ph].

[81] Eugenio Megias, Giuliano Panico, Oriol Pujolas, Mariano Quiros, A natural origin for the LHCb anomalies, J. High Energy Phys. 09 (2016) 118, https://doi.org/10.1007/JHEP09(2016)118, arXiv:1608.02362 [hep-ph].

[82] Isabel Garcia Garcia, LHCb anomalies from a natural perspective, J. High Energy Phys. 03 (2017) 040, https://doi.org/10.1007/JHEP03(2017)040, arXiv:1611.03507 [hep-ph].

[83] P. Ko, Yuji Omura, Yoshihiro Shigekami, Chaehyun Yu, LHCb anomaly and B physics in flavored Z' models with flavored Higgs doublets, Phys. Rev. D 95 (11) (2017) 115040, https://doi.org/10.1103/PhysRevD.95.115040, arXiv:1702.08666 [hep-ph].

[84] Eugenio Megias, Mariano Quiros, Lindber Salas, Lepton-flavor universality violation in R_K and $R_{D^{(*)}}$ from warped space, J. High Energy Phys. 07 (2017) 102, https://doi.org/10.1007/JHEP07(2017)102, arXiv:1703.06019 [hep-ph].

[85] Ashutosh Kumar Alok, Neetu Raj Singh Chundawat, Shireen Gangal, Dinesh Kumar, A global analysis of $b \to s \ell \ell$ data in heavy and light Z' models, Eur. Phys. J. C 82 (10) (2022) 967, https://doi.org/10.1140/epjc/s10052-022-10816-w, arXiv:2203.13217 [hep-ph].

[86] Allanach Ben, Anna Mullin, Plan B: new Z' models for b → $s\ell^+\ell^-$ anomalies, J. High Energy Phys. 09 (2023) 173, https://doi.org/10.1007/JHEP09(2023)173, arXiv:2306.08669 [hep-ph].

[87] Ben Gripaios, Composite leptoquarks at the LHC, J. High Energy Phys. 02 (2010) 045, https://doi.org/10.1007/JHEP02(2010)045, arXiv:0910.1789 [hep-ph].

[88] Ben Gripaios, Marco Nardecchia, S.A. Renner, Composite leptoquarks and anomalies in B-meson decays, J. High Energy Phys. 05 (2015) 006, https://doi.org/10.1007/JHEP05(2015)006, arXiv:1412.1791 [hep-ph].

[89] Ivode Medeiros Varzielas, Gudrun Hiller, Clues for flavor from rare lepton and quark decays, J. High Energy Phys. 06 (2015) 072, https://doi.org/10.1007/JHEP06(2015)072, arXiv:1503.01084 [hep-ph].

[90] Andreas Crivellin, Dario Müller, Toshihiko Ota, Simultaneous explanation of $R(D^{(*)})$ and $b \to s\mu^+ \mu^-$: the last scalar leptoquarks standing, J. High Energy Phys. 09 (2017) 040, https://doi.org/10.1007/JHEP09(2017)040, arXiv:1703.09226 [hep-ph].

[91] Suchismita Sahoo, Rukmani Mohanta, Scalar leptoquarks and the rare B meson decays, Phys. Rev. D 91 (9) (2015) 094019, https://doi.org/10.1103/PhysRevD.91.094019, arXiv:1501.05193 [hep-ph].

[92] Rodrigo Alonso, Benjamín Grinstein, Jorge Martin Camalich, Lepton universality violation and lepton flavor conservation in B-meson decays, J. High Energy Phys. 10 (2015) 184, https://doi.org/10.1007/JHEP10(2015)184, arXiv:1505.05164 [hep-ph].

[93] Riccardo Barbieri, Gino Isidori, Andrea Pattori, Fabrizio Senia, Anomalies in B-decays and $U(2)$ flavour symmetry, Eur. Phys. J. C 76 (2) (2016) 67, https://doi.org/10.1140/epjc/s10052-016-3905-3, arXiv:1512.01560 [hep-ph].

[94] Damir Bečirević, Svjetlana Fajfer, Nejc Košnik, Olcyr Sumensari, Leptoquark model to explain the B-physics anomalies, R_K and R_D, Phys. Rev. D 94 (11) (2016) 115021, https://doi.org/10.1103/PhysRevD.94.115021, arXiv:1608.08501 [hep-ph].

[95] Yi Cai, John Gargalionis, Michael A. Schmidt, Raymond R. Volkas, Reconsidering the one leptoquark solution: flavor anomalies and neutrino mass, J. High Energy Phys. 10 (2017) 047, https://doi.org/10.1007/JHEP10(2017)047, arXiv:1704.05849 [hep-ph].

[96] Suchismita Sahoo, Rukmani Mohanta, Anjan K. Giri, Explaining the R_K and $R_{D^{(*)}}$ anomalies with vector leptoquarks, Phys. Rev. D 95 (3) (2017) 035027, https://doi.org/10.1103/PhysRevD.95.035027, arXiv:1609.04367 [hep-ph].

[97] Riccardo Barbieri, Christopher W. Murphy, Fabrizio Senia, B-decay anomalies in a composite leptoquark model, Eur. Phys. J. C 77 (1) (2017) 8, https://doi.org/10.1140/epjc/s10052-016-4578-7, arXiv:1611.04930 [hep-ph].

[98] Dario Buttazzo, Admir Greljo, Gino Isidori, David Marzocca, B-physics anomalies: a guide to combined explanations, J. High Energy Phys. 11 (2017) 044, https://doi.org/10.1007/JHEP11(2017)044, arXiv:1706.07808 [hep-ph].

[99] Joydeep Roy, Probing leptoquark chirality via top polarization at the colliders, arXiv:1811.12058 [hep-ph], Nov. 2018.

[100] David Marzocca, Addressing the B-physics anomalies in a fundamental composite Higgs model, J. High Energy Phys. 07 (2018) 121, https://doi.org/10.1007/JHEP07(2018)121, arXiv:1803.10972 [hep-ph].

[101] Damir Bečirević, Ilja Doršner, Svjetlana Fajfer, Nejc Košnik, Darius A. Faroughy, Olcyr Sumensari, Scalar leptoquarks from grand unified theories to accommodate the B-physics anomalies, Phys. Rev. D 98 (5) (2018) 055003, https://doi.org/10.1103/PhysRevD.98.055003, arXiv:1806.05689 [hep-ph].

[102] Natascia Vignaroli, Seeking leptoquarks in the $\mathbf{t\bar{t}}$ plus missing energy channel at the high-luminosity LHC, Phys. Rev. D 99 (3) (2019) 035021, https://doi.org/10.1103/PhysRevD.99.035021, arXiv:1808.10309 [hep-ph].

[103] Natascia Vignaroli, Leptoquarks in B-meson anomalies: simplified models and HL-LHC discovery prospects, in: G. D'Ambrosio, G. De Nardo (Eds.), Nuovo Cimento C 43 (2–3) (2020) 53, https://doi.org/10.1393/ncc/i2020-20053-0, arXiv:1912.00899 [hep-ph].

[104] P.S. Bhupal Dev, Rukmani Mohanta, Sudhanwa Patra, Suchismita Sahoo, Unified explanation of flavor anomalies, radiative neutrino masses, and ANITA anomalous events in a vector leptoquark model, Phys. Rev. D 102 (9) (2020) 095012, https://doi.org/10.1103/PhysRevD.102.095012, arXiv:2004.09464 [hep-ph].

[105] Andreas Crivellin, Benjamin Fuks, Luc Schnell, Explaining the hints for lepton flavour universality violation with three S_2 leptoquark generations, J. High Energy Phys. 06 (2022) 169, https://doi.org/10.1007/JHEP06(2022)169, arXiv:2203.10111 [hep-ph].

[106] A. Angelescu, Damir Bečirević, D.A. Faroughy, O. Sumensari, Closing the window on single leptoquark solutions to the B-physics anomalies, J. High Energy Phys. 10 (2018) 183, https://doi.org/10.1007/JHEP10(2018)183, arXiv:1808.08179 [hep-ph].

[107] Andrei Angelescu, Damir Bečirević, Darius A. Faroughy, Florentin Jaffredo, Olcyr Sumensari, Single leptoquark solutions to the B-physics anomalies, Phys. Rev. D 104 (5) (2021) 055017, https://doi.org/10.1103/PhysRevD.104.055017, arXiv:2103.12504 [hep-ph].

[108] Lukas Allwicher, Damir Becirevic, Gioacchino Piazza, Salvador Rosauro-Alcaraz, Olcyr Sumensari, Understanding the first measurement of $\mathcal{B}(B \to K \nu \bar{\nu})$, arXiv:2309.02246 [hep-ph], Sept. 2023.

[109] R. Glattauer, et al., Measurement of the decay $B \to D \ell \nu_\ell$ in fully reconstructed events and determination of the Cabibbo-Kobayashi-Maskawa matrix element $|V_{cb}|$, Phys. Rev. D 93 (3) (2016) 032006, https://doi.org/10.1103/PhysRevD.93.032006, arXiv:1510.03657 [hep-ex].

[110] Aubert Bernard, et al., Measurement of |V(cb)| and the form-factor slope in anti-B —> D l- anti-nu decays in events tagged by a fully reconstructed B meson, Phys. Rev. Lett. 104 (2010) 011802, https://doi.org/10.1103/PhysRevLett.104.011802, arXiv:0904.4063 [hep-ex].

[111] W. Dungel, et al., Measurement of the form factors of the decay B0 -> D*- ell+ nu and determination of the CKM matrix element |Vcb|, Phys. Rev. D 82 (2010) 112007, https://doi.org/10.1103/PhysRevD.82.112007, arXiv:1010.5620 [hep-ex].

[112] A. Abdesselam, et al., Precise determination of the CKM matrix element V_{cb} with $\bar{B} \to D^{*+} \ell^- \bar{\nu}_\ell$ decays with hadronic tagging at Belle, arXiv:1702.01521 [hep-ex], Feb. 2017.

[113] Karol Adamczyk, Semitauonic B decays at Belle/Belle II, in: 10th International Workshop on the CKM Unitarity Triangle, Jan. 2019, arXiv:1901.06380 [hep-ex].

[114] Y. Amhis, et al., Averages of b-hadron, c-hadron, and τ-lepton properties as of summer 2016, Eur. Phys. J. C 77 (12) (2017) 895, https://doi.org/10.1140/epjc/s10052-017-5058-4, arXiv:1612.07233 [hep-ex].
[115] Aubert Bernard, et al., Measurements of the semileptonic decays anti-B —> D l anti-nu and anti-B —> D* l anti-nu using a global fit to D X l anti-nu final states, Phys. Rev. D 79 (2009) 012002, https://doi.org/10.1103/PhysRevD.79.012002, arXiv:0809.0828 [hep-ex].
[116] Aubert Bernard, et al., Determination of the form-factors for the decay $B^0 \to D^{*-}\ell^+\nu_l$ and of the CKM matrix element $|V_{cb}|$, Phys. Rev. D 77 (2008) 032002, https://doi.org/10.1103/PhysRevD.77.032002, arXiv:0705.4008 [hep-ex].
[117] Aubert Bernard, et al., A measurement of the branching fractions of exclusive $\bar{B} \to D^{(*)}$ (π) $\ell^-\bar{\nu}(\ell^)$ decays in events with a fully reconstructed B meson, Phys. Rev. Lett. 100 (2008) 151802, https://doi.org/10.1103/PhysRevLett.100.151802, arXiv:0712.3503 [hep-ex].
[118] Aubert Bernard, et al., Measurement of the decay $B^- \to$ D*0 $e^-\bar{\nu}(e)$, Phys. Rev. Lett. 100 (2008) 231803, https://doi.org/10.1103/PhysRevLett.100.231803, arXiv:0712.3493 [hep-ex].